Tissue flow regulates planar cell polarity independently of the Frizzled core pathway

Cell Reports

Article

Tissue flow regulates planar cell polarity independently of the Frizzled core pathway

Graphical abstract

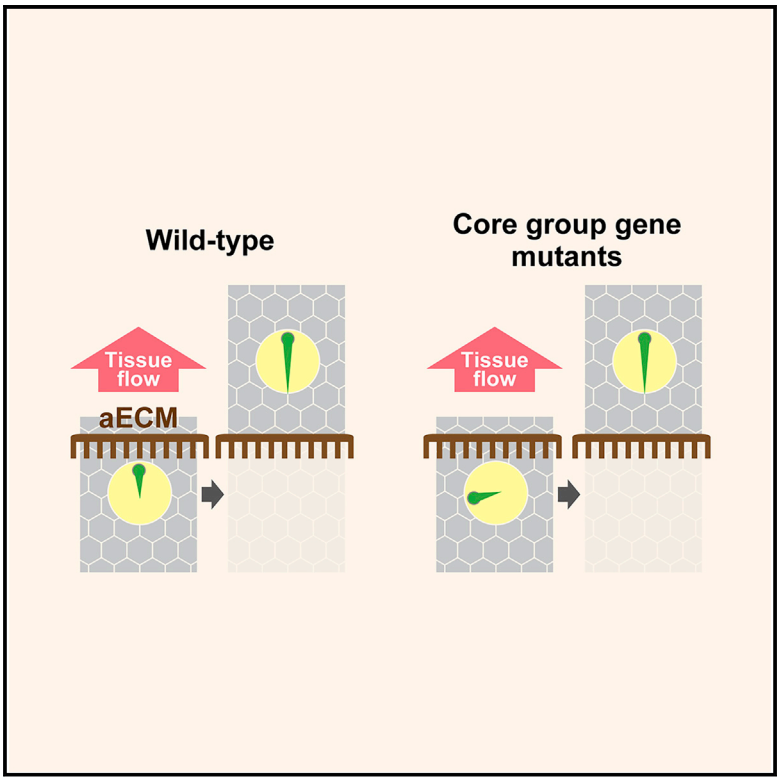

Highlights

- Core group mutants only slightly affect bristle polarity in the central notum
- This near-normal PCP results from tissue flow-mediated rescue during development
- Tissue flow can orient bristles in the opposite direction to the flow
- The aECM acts like a "comb" to align bristles independently of the core group

Authors

Tomonori Ayukawa, Masakazu Akiyama, Yasukazu Hozumi, ..., Haruki Senoo, Takehiko Sasaki, Masakazu Yamazaki

Correspondence

yamazaki@med.akita-u.ac.jp

In brief

For the last several decades, it has been thought that there might be other PCP mechanisms that are independent of the core group, but their underlying mechanisms remain unclear. In this study, Ayukawa et al. show that tissue flow is a mechanism governing core group-independent PCP on the *Drosophila* notum.

Ayukawa et al., 2022, Cell Reports *40*, 111388
September 20, 2022
https://doi.org/10.1016/j.celrep.2022.111388

CellPress

Cell Reports

CellPress
OPEN ACCESS

Article

Tissue flow regulates planar cell polarity independently of the Frizzled core pathway

Tomonori Ayukawa,[1] Masakazu Akiyama,[2,3] Yasukazu Hozumi,[1] Kenta Ishimoto,[4] Junko Sasaki,[5] Haruki Senoo,[1] Takehiko Sasaki,[5] and Masakazu Yamazaki[1,6,7,*]

[1]Department of Cell Biology and Morphology, Akita University Graduate School of Medicine, Akita 010-8543, Japan
[2]Meiji Institute for Advanced Study of Mathematical Sciences, Meiji University, Tokyo 164-8525, Japan
[3]Faculty of Science, Academic Assembly, University of Toyama, Toyama 930-8555, Japan
[4]Research Institute for Mathematical Sciences, Kyoto University, Kyoto 606-8502, Japan
[5]Department of Biochemical Pathophysiology, Medical Research Institute, Tokyo Medical and Dental University, Tokyo 113-8510, Japan
[6]Japan Science and Technology Agency, PRESTO, Saitama 332-0012, Japan
[7]Lead contact
*Correspondence: yamazaki@med.akita-u.ac.jp
https://doi.org/10.1016/j.celrep.2022.111388

SUMMARY

Planar cell polarity (PCP) regulates the orientation of external structures. A core group of proteins that includes Frizzled forms the heart of the PCP regulatory system. Other PCP mechanisms that are independent of the core group likely exist, but their underlying mechanisms are elusive. Here, we show that tissue flow is a mechanism governing core group-independent PCP on the *Drosophila* notum. Loss of core group function only slightly affects bristle orientation in the adult central notum. This near-normal PCP results from tissue flow-mediated rescue of random bristle orientation during the pupal stage. Manipulation studies suggest that tissue flow can orient bristles in the opposite direction to the flow. This process is independent of the core group and implies that the apical extracellular matrix functions like a "comb" to align bristles. Our results reveal the significance of cooperation between tissue dynamics and extracellular substances in PCP establishment.

INTRODUCTION

Many epithelial tissues show a coordinated polarity of cells in the tissue plane that is orthogonal to the axis of apico-basal polarity. This phenomenon is referred to as planar cell polarity (PCP) (Adler, 2002; Lawrence and Casal, 2018). PCP is manifested in external structures on the body surface (e.g., animal hairs) and in the cellular appendages of internal organs (e.g., the stereocilia in the inner ear). The polarization of these features plays a crucial role in numerous functions, such as hearing and left-right axis determination (Axelrod, 2020; Butler and Wallingford, 2017; Devenport, 2014). PCP also coordinates multicellular behaviors that include convergent extension and oriented cell division, and aberrant regulation of PCP is implicated in human pathologies (Simons and Mlodzik, 2008).

In *Drosophila*, PCP is obvious in several different body regions, including the wing, covered by distally pointing hairs, and the notum, decorated with posteriorly pointing bristles. Genetic studies in *Drosophila* focusing on polarized structures have identified a set of evolutionarily conserved genes called the "core group" that are required for PCP (Adler, 2002; Gubb and Garcia-Bellido, 1982). The core group consists of the cell surface transmembrane proteins Frizzled (Fz) (Vinson et al., 1989), Strabismus (Stbm, also known as Van Gogh) (Taylor et al., 1998; Wolff and Rubin, 1998), and Flamingo (Fmi, also known as Starry Night) (Chae et al., 1999; Usui et al., 1999), as well as the cytoplasmic components Dishevelled (Dsh) (Klingensmith et al., 1994; Theisen et al., 1994), Prickle (Pk) (Gubb et al., 1999), and Diego (Dgo) (Feiguin et al., 2001). Both in *Drosophila* and vertebrate tissues, the core group proteins are recruited to the opposite sides of each cell, where they assemble into asymmetric apicolateral complexes (Axelrod, 2001; Bastock et al., 2003; Feiguin et al., 2001; Goodrich and Strutt, 2011; Jenny et al., 2003; Shimada et al., 2001; Strutt, 2001; Tree et al., 2002; Usui et al., 1999). For example, in each *Drosophila* wing cell, Fz, Dsh, and Dgo are localized at the distal side, whereas Stbm and Pk are localized at the proximal side, with Fmi residing on both sides. This asymmetry is achieved by intracellular mutual repulsion and intercellular preferential interaction between the Fz-Dsh-Dgo-Fmi and Stbm-Pk-Fmi complexes (Amonlirdviman et al., 2005; Bastock et al., 2003; Chen et al., 2008; Das et al., 2004; Jenny et al., 2003; Strutt and Strutt, 2008; Tree et al., 2002; Wu and Mlodzik, 2008). All core group proteins are physically and/or functionally interconnected, and loss of any one of them abolishes the asymmetric localization of the rest, leading to disorganized external structures (Goodrich and Strutt, 2011; McNeill, 2010; Uemura and Shimada, 2003; Zallen, 2007). Similarly, vertebrate orthologs of core group proteins are critical for PCP regulation in these species (Simons and Mlodzik, 2008).

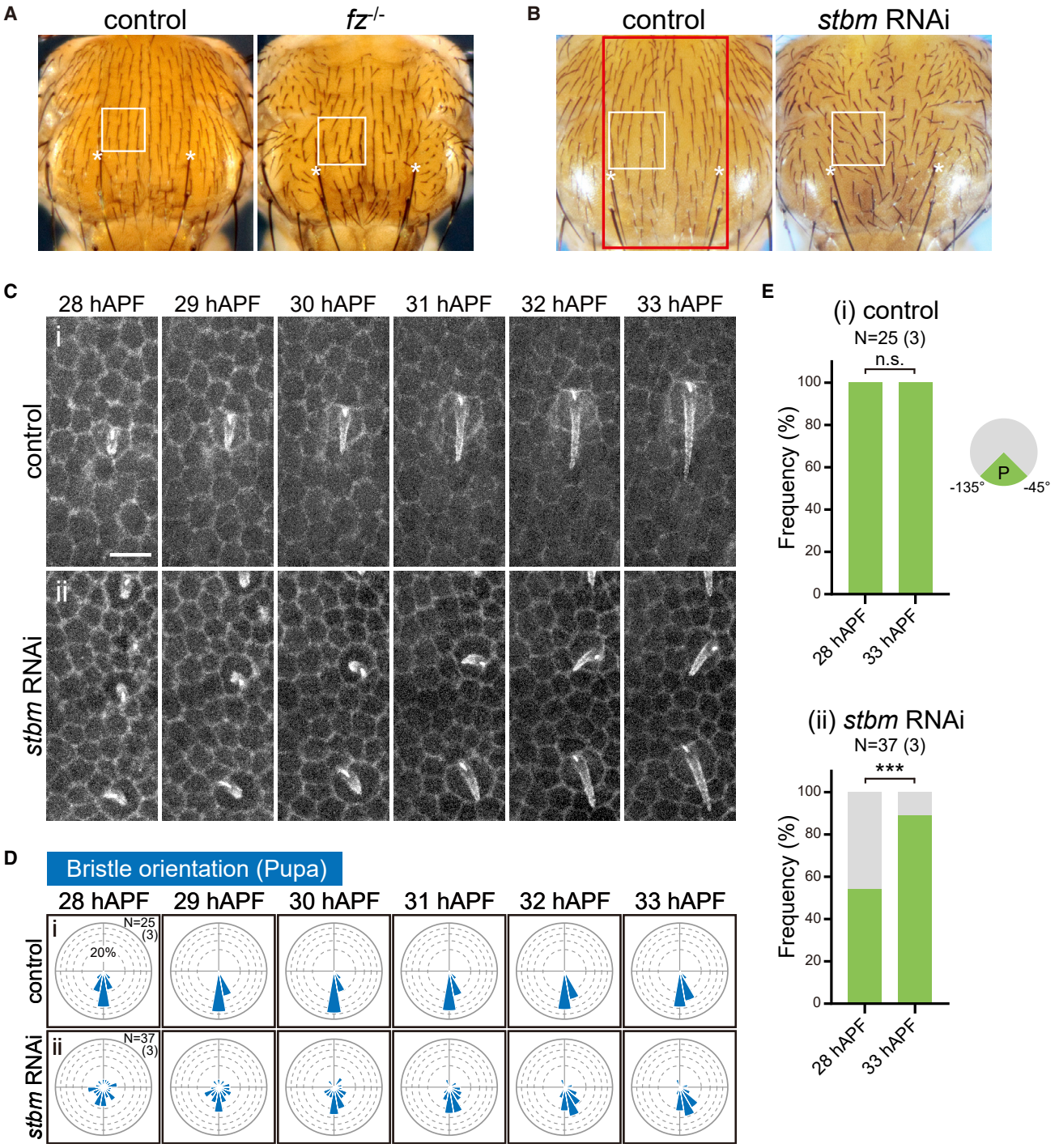

Figure 1. The notum bristle orientation defect caused by PCP core group gene inactivation is rescued by an unknown mechanism during pupal development

(A) Macroscopic dorsal views of the nota of adult (left) control and (right) *fz* mutant ($fz^{-/-}$) flies. The boxed area is the "A region" analyzed for all flies in this study unless otherwise stated. *aDC bristle. In all figures, the anterior direction is to the top and the posterior direction is to the bottom unless otherwise stated.

(B) Macroscopic dorsal views of the nota of adult (left) *pannier* (*pnr*)-Gal4 (control), and (right) *pnr*-Gal4>UAS-*stbm*-IR (*stbm* RNAi) flies. The area of *pnr*-Gal4 expression is indicated by the red box. The A region is also shown.

(C) Time-lapse live imaging of developing bristles labeled with sGMCA in the A regions of (i) control and (ii) *stbm* RNAi pupae. Bristles are shown at the indicated number of hours after puparium formation (hAPF). Scale bar, 10 μm.

(legend continued on next page)

Despite the critical nature of the PCP core group, it has long been thought that other PCP regulatory mechanisms that are independent of the core group may exist (Adler et al., 1987; Adler, 2002; Casal et al., 2006; Donoughe and DiNardo, 2011; Gubb and Garcia-Bellido, 1982; Jones et al., 1996; Olguin et al., 2011; Shulman et al., 1998). Even in the *Drosophila* wing, null mutations in core group genes disrupt hair orientation but do not cause complete loss of polarity control. In large areas of these mutant wings, the hairs are not randomly oriented but instead point in the same (abnormal) direction in a coordinated fashion. This lack of randomness demonstrates that a core group-independent mechanism can also act to align hairs (if not determine their proper direction). Similar phenomena have been reported in mammalian tissues but their molecular underpinnings remain enigmatic (Cetera et al., 2017; Copley et al., 2013).

To elucidate molecular mechanisms governing core group-independent PCP, we have studied *Drosophila* notum bristles, which are only slightly affected by loss of core group function (Adler, 2002; Lu et al., 1999; Feiguin et al., 2001). Notum bristles are derived from a single sensory organ precursor (SOP) cell through a series of asymmetric cell divisions that result in two daughter cells acquiring different cell fates (Bellaiche and Schweisguth, 2001; Betschinger and Knoblich, 2004). During SOP division, the mitotic spindle is oriented along the anterior-posterior axis by the action of the core group proteins, and the cell-fate determinant Numb is segregated into only one of the two daughter cells. These two cells then divide asymmetrically to produce all four cell types (including the bristle cell) that make up the external sensory (ES) organ (Bellaiche and Schweisguth, 2001; Betschinger and Knoblich, 2004). Core group mutants show random spindle orientation but not random bristle orientation (Bellaiche et al., 2001; Gho and Schweisguth, 1998; Lu et al., 1999), suggesting that an unknown mechanism also contributes to notum bristle orientation.

A genetic analysis of the PCP gene *chascon* (*chas*) has demonstrated that external forces can perturb bristle orientation in the *Drosophila* notum independently of the core group (Olguin et al., 2011). Loss of function of *chas* results in defective tissue resistance to the mechanical pulling force mediated by the indirect flight muscles (IFMs). Thus, the ability of a tissue to adapt to external forces appears critical for maintaining PCP in the notum. However, it remains unclear whether and how such external forces positively affect notal PCP formation independently of the core group.

RESULTS

Core group-independent rescue of bristle orientation defects during pupal development

Loss-of-function mutations in core group genes only slightly affect *Drosophila* notum bristles (mainly in the central region) and do not randomize their orientation (Adler, 2002; Feiguin et al., 2001; Lu et al., 1999; Wolff and Rubin, 1998). The same weak PCP phenotype appears after tissue-specific RNAi-mediated knockdown of a core PCP gene (Brand and Perrimon, 1993; Mummery-Widmer et al., 2009; Olguin et al., 2011). We confirmed these previous results by comparing the nota of control *Drosophila* with those of *fz* mutant flies ($fz^{-/-}$) (Figure 1A), as well as transgenic flies depleted of *stbm* function due to knockdown by *stbm* RNAi (Figure 1B). These two strains, equivalent in phenotype, gave us the tools to perform our mechanistic studies.

First, we crossed our control and transgenic RNAi flies to the sGMCA line, which expresses the green fluorescent protein (GFP)-tagged actin-binding domain of Moesin under the control of the *spaghetti squash* promoter (Kiehart et al., 2000). We then monitored bristle formation on the nota of these animals using a live imaging system. The anterior dorsocentral (aDC) bristle was used as a positional landmark, facilitating efficient imaging of a central notum region anterior to the aDC bristle (designated the "A region") (Figure 1A, white box). We focused on the developmental stage starting from 28 h after puparium formation (hAPF) to 33 hAPF because the bristles start to sprout at around 27–28 hAPF. In control pupae, the bristles sprouted in the posterior direction and then elongated posteriorly, as expected (Figures 1Ci, 1Di, and 1Ei; Video S1). In contrast, in *stbm* RNAi pupae, the bristles on the notum sprouted in random directions. Interestingly, this orientation defect was gradually rescued over time, resulting in properly posteriorly oriented bristles by 32 hAPF (Figures 1Cii, 1Dii, and 1Eii; Video S2). Thus, the core group initially plays a crucial role in regulating notum bristle orientation, but an unknown mechanism that is independent of the core group can later rescue bristle orientation defects caused by loss of core group function.

Normal orientation of tissue flow in a core group gene mutant

In wild-type nota, epithelial cells flow anteriorly during the pupal stage (21–36 hAPF) (Bosveld et al., 2012). To examine tissue flow in nota lacking a core group gene, we performed live imaging studies of control and *fz* mutant notum epithelial cells expressing E-cadherin::GFP (Huang et al., 2009). We tracked tissue flow in the A region of control and *fz* mutant nota by focusing on socket cells, which, like bristle cells, are constituents of the ES organs (Figures 2A and 2B). We then analyzed the angle and velocity of tissue flow from 24 to 34 hAPF in control and *fz* mutant nota. In controls, notum epithelial cells flowed anteriorly (Figures 2Ci and 2Di; Video S3), with gradually decreasing velocity over time (Figure S1Ai). Loss of *fz* had little influence on the angle of tissue flow (Figures 2Cii and 2Dii; Video S3), but slightly decreased flow velocity compared with controls (Figure S1Aiii). The same phenotypes were observed in *stbm* RNAi nota

(D) Quantification of the results in (C). Rose diagrams show the angular distribution of the bristles in (i) control and (ii) *stbm* RNAi pupae at the indicated times (see the STAR Methods).

(E) Statistical analysis of the results in (D). The proportion of bristles pointing to either the posterior direction (P) or to any other direction are indicated in green and gray, respectively, in (i) control and (ii) *stbm* RNAi pupae at the indicated times. ***$p < 0.005$ by Fisher's exact test.

See also Videos S1 and S2.

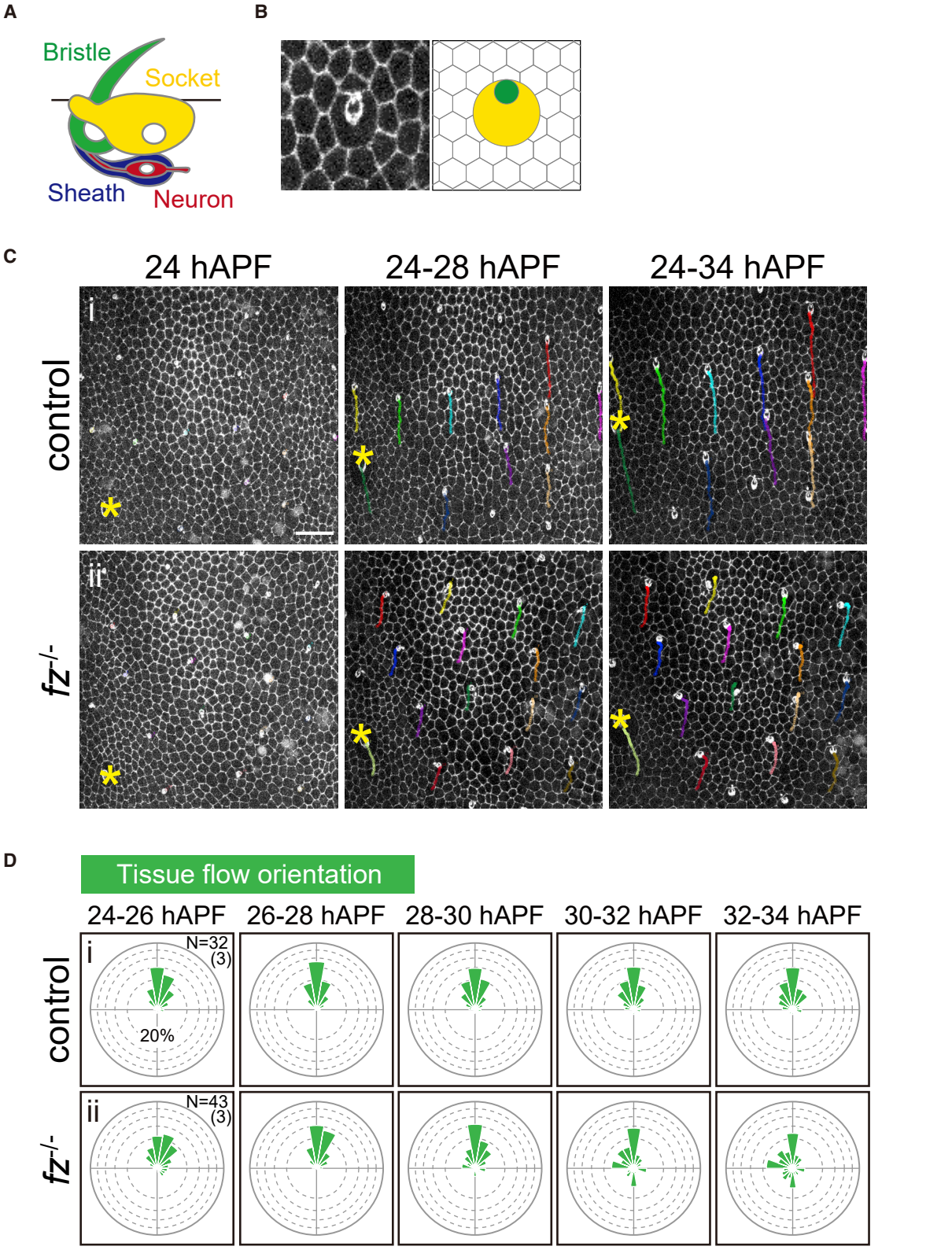

(legend on next page)

(Figures S2A, S2A′, S2B, S2B′, S2Ei, S2Eii, S2Fi, S2Fiii, S3i, and S3iii; Video S4). These data suggest that the PCP core group genes are not responsible for tissue flow orientation in the A region of the *Drosophila* notum.

Bristles are oriented in the direction opposite to tissue flow regardless of absolute tissue flow direction

We speculated that bristles are oriented in the direction opposite to that of the notal tissue flow in a manner independent of PCP core group function. To test this hypothesis, we employed a genetic manipulation approach in which double loss of either *chas* or *jitterbug* (*jbug*) plus a core group gene reverses the direction of notal PCP (Olguin et al., 2011). Jbug is the *Drosophila* ortholog of the actin-binding factor Filamin, and Chas is a Jbug-binding protein; both have been tagged as PCP regulators in previous genetic screens (Mummery-Widmer et al., 2009; Olguin et al., 2011). Chas cooperates with Jbug to maintain PCP on the *Drosophila* notum by balancing the forces of mechanical stress (Olguin et al., 2011). A double loss of function of *chas* plus a core group gene, such as *fz*, *stbm*, *fmi*, or *pk*, reverses bristle orientation in the A region of the notum (Olguin et al., 2011), a phenotype we confirmed by using mutants and RNAi-mediated knockdown of *chas* and *fz* (or *stbm*) (Figures 3Ai–iv, 3Ai'–iv', S2A–S2D, and S2A′–S2D′).

If epithelial cell flow is responsible for PCP reversal in flies lacking *chas* plus a core group gene, tissue flow orientation in these animals should be reversed. During 24–28 hAPF, cells in the A region of *chas*, *fz* mutants or *chas*, *stbm* RNAi pupae began to flow anteriorly and then laterally, becoming mainly posteriorly directed by 28–30 hAPF (Figures 3Bi, 3Ci, S2Eiv, and S3vii; Videos S3 and S4). These results support the idea that bristles are oriented in the direction opposite to that of the notal tissue flow in a manner that is independent of core group function. We also found that, in the A regions of *chas*, *fz* mutants (or *chas*, *stbm* RNAi pupae) compared with controls, the decrease in flow velocity over time was milder (Figures S1Ai, S1Av, S2Fi, and S2Fvii). Intriguingly, even on the same *chas*, *stbm* RNAi pupae, the orientation of tissue flow was near random during 28–32 hAPF in a central notum region posterior to the aDC bristle (designated the "P region"), which is consistent with the fact that bristles in the P region of adult flies were oriented in various directions without reversion (Figures S2D, S2D", S2Eiv, and S3viii). This phenomenon, in which bristle orientation is opposite to that of tissue flow, was also observed in control, *fz* mutant, and *chas* RNAi pupae (compare Figure 2Di versus Figures 3Ai and 3Ai'; Figure 2Dii versus Figures 3Aiii and 3Aiii'; Figures S2A–S2D" versus Figure S3). Taken together, these results suggested that the orientation of bristles is opposite to that of tissue flow in the notum, regardless of tissue flow direction.

Unlike in the notum central region, in the notum lateral region, loss of core group function results in highly abnormal bristle orientation in adult flies (Adler, 2002; Lu et al., 1999; Wolff and Rubin, 1998). We found that, in control nota, the epithelial cells in the lateral region flowed anteriorly (like cells in the central region), although this flow velocity was slightly slower than that in the central region (Figures S4Ai, S4Bi, S4Bii, S4Ci, and S4Cii). However, in *fz* mutant nota, unlike cells in the central region, lateral region epithelial cells flowed toward the midline of the pupae during 24–28 hAPF, with cells flowing back toward the lateral side after this time (Figures S4Aii, S4Biii, and S4Biv). Consistent with the flow direction after 28 hAPF, bristles in the lateral region of *fz* mutant nota tended to orient toward the midline (Figure 3Aiii), supporting the idea that bristles are oriented in the direction opposite to that of notal tissue flow. Lateral region flow velocity in *fz* mutant nota was only slightly slower than that in the central region (Figures S4Ciii and S4Civ). Thus, this abnormal tissue flow might be the reason why the PCP defect in the lateral region of core group mutants is not rescued.

Effects of tissue flow manipulation on bristle orientation

To further investigate whether tissue flow was a key force regulating bristle orientation, we next tried to manipulate the orientation of the reversed tissue flow in *chas*, *fz* double mutants. To achieve this objective, we focused on the IFMs (Figure S4D). The IFMs consist of the dorsal-longitudinal flight muscles, which are oriented from anterior to posterior, and the dorso-ventral muscles (DVMs), which are oriented from dorsal to ventral (Fernandes et al., 1991). These muscles attach to notum epithelial cells called "tendon cells." During PCP establishment at the pupal stage, the IFMs shorten to generate mechanical force and then pull the epithelium at the attachment sites. When *chas* is inactivated, this IFM-generated mechanical stress causes notum bristle orientation defects (Olguin et al., 2011; Vega-Macaya et al., 2016), a finding we confirmed (Figures 3Aii and 3Aii').

We hypothesized that the mechanical pulling force generated by the IFMs might cause the reversed tissue flow in *chas*, *fz* mutants. We removed this mechanical pulling force by genetically ablating the IFMs through overexpression of a constitutively activated form of the Notch receptor (N^{act}) in muscle progenitor cells (*1151*-Gal4>N^{act}) (Olguin et al., 2011). We found that IFM ablation changed the cell flow orientation from the reverse (posterior) direction to the normal (anterior) direction (Figures 3Bii, 3Cii, and S1; Video S5). On the other hand, IFM ablation had little impact

Figure 2. Normal orientation of tissue flow on the notum of a core group gene mutant

(A) Schematic diagram of the *Drosophila* external sensory (ES) organ showing its component bristle cell (green), socket cell (yellow), neuron (red), and sheath cell (blue).

(B) Left: dorsal image of an ES organ surrounded by epithelial cells on the notum of a wild-type pupa expressing E-cadherin::GFP. Right: schematic diagram of the image in the left panel. Bristle cell, green; socket cell, yellow; epithelial cells, colorless.

(C) Trajectories of the socket cells in the region boxed in Figure 1A (A region) in (i) control and (ii) $fz^{-/-}$ pupae expressing E-cadherin::GFP. Left panels, the position of the socket cells at 24 hAPF; middle panels, trajectories of the socket cells during 24–28 hAPF; right panels, trajectories of the socket cells during 24–34 hAPF. *left aDC macrochaetae. Scale bar, 20 μm.

(D) Quantification of the results in (C). Rose diagrams show the angles of the movements of socket cells during each indicated 2 h window in (i) control and (ii) $fz^{-/-}$ pupae. Angles were measured between consecutive frames of each time-lapse series at 10 min intervals.

See also Figures S1, S2, and S3 and Videos S3 and S4.

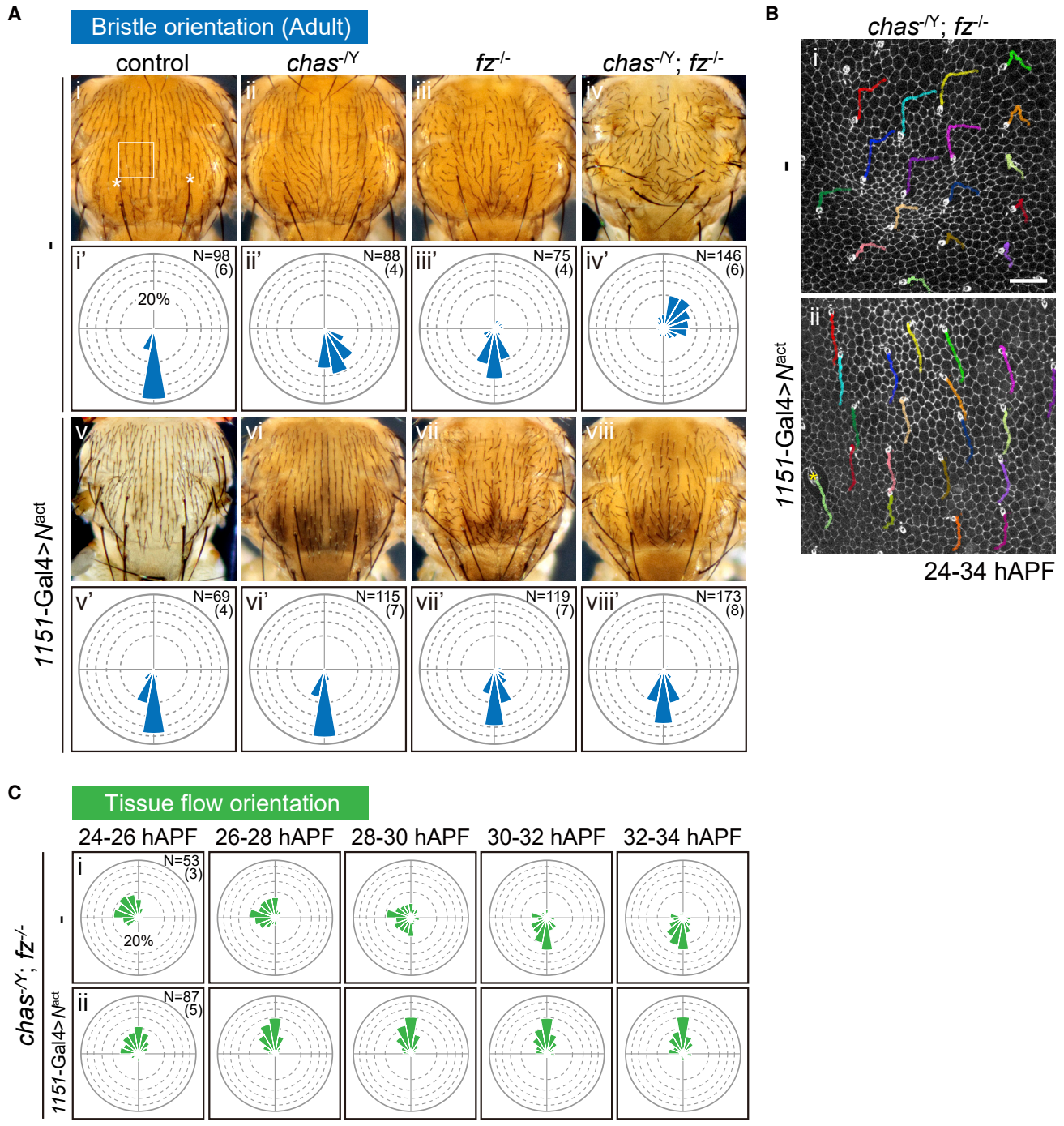

Figure 3. Tissue flow orients bristles in the opposite direction

(A) (i–viii) Macroscopic dorsal views of notal bristle phenotypes in adult (i) control flies and (ii–iv) flies deficient in the indicated PCP genes, as well as (v) control flies and (vi–viii) the same mutant strains subjected to IFM ablation (*1151*-Gal4>N^{act}). *aDC bristle. (i'–viii') Rose diagrams showing the angular distribution of the bristles in the A region (white box in control (i)) of the nota in (i–viii).

(B) Trajectories (24–34 hAPF) of socket cells in the A regions of E-cadherin::GFP-labeled notum epithelium in (i) $chas^{-/Y}$;$fz^{-/-}$ pupae and (ii) $chas^{-/Y}$;$fz^{-/-}$ pupae subjected to IFM ablation (*1151*-Gal4>N^{act}). *left aDC macrochaetae. Scale bar, 20 μm.

(C) Quantification of the results in (B). Rose diagrams showing the angles of the movements of socket cells in $chas^{-/Y}$;$fz^{-/-}$ pupae (i) without (–) and (ii) with IFM ablation (*1151*-Gal4>N^{act}). Angles were measured between consecutive frames of each time-lapse series at 10 min intervals.

See also Figures S1, S2, S3, and S4; Videos S3, S4, and S5.

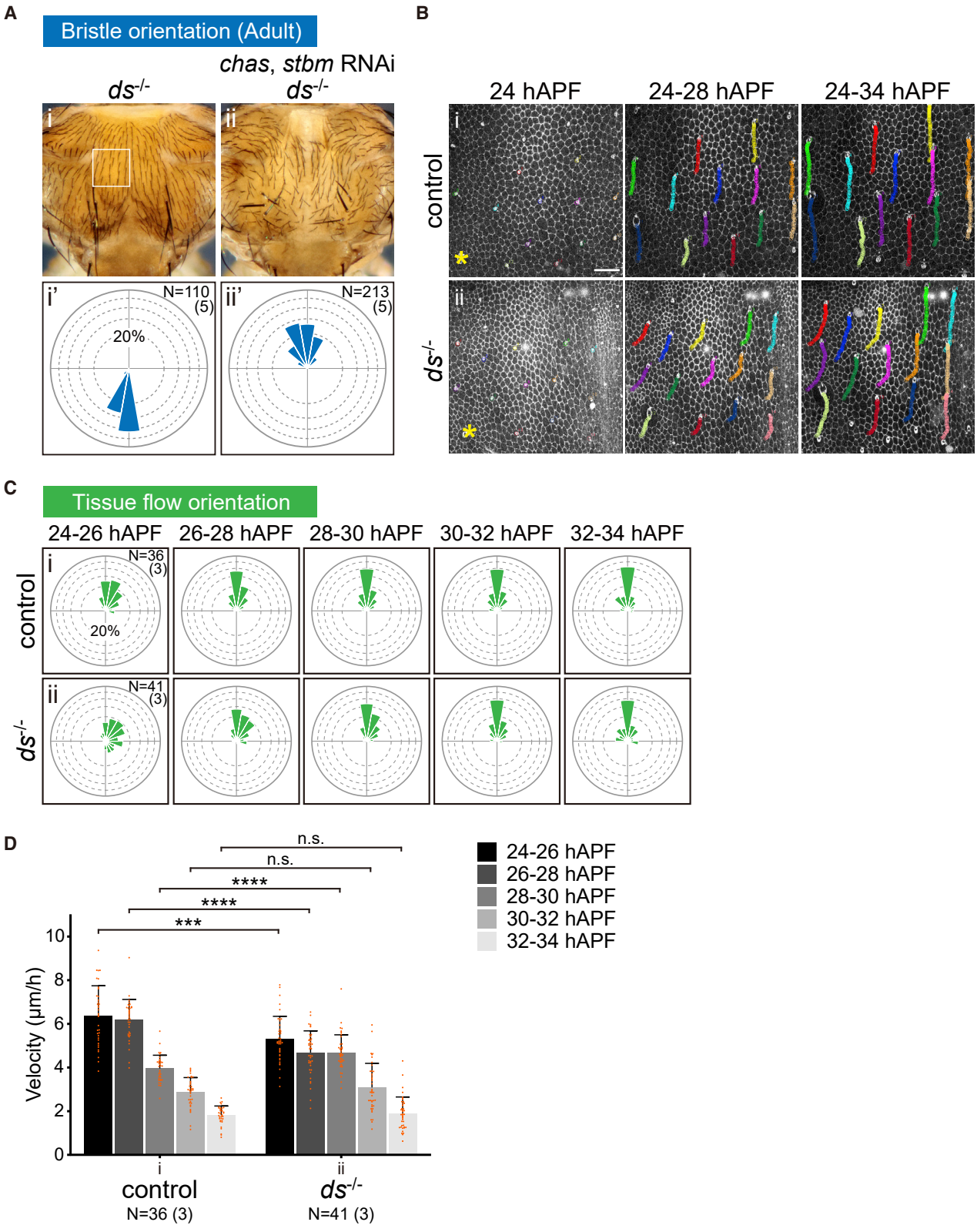

(legend on next page)

on cell flow direction in control or *fz* mutant pupae (Figure S1; Video S5), although this manipulation had slightly increased flow velocity in both strains by the end of the observation period (Figures S1Aii and S1Aiv). Thus, the pulling force generated by IFMs can reverse tissue flow in *chas*, *fz* mutants but is not responsible for the normal flow in control and *fz* mutant animals.

Consistent with the above data, IFM ablation completely suppressed the PCP reversal phenotype in adult *chas*, *fz* mutant nota (Figures 3Aviii and 3Aviii'), resulting in near-normal bristle orientation in the A region; this phenotype resembled that of the *fz* mutant (Figures 3Aiii and 3Aiii'). The same suppressive effect on PCP reversal was observed when IFM mechanical pulling force was removed by knocking down the *kon-tiki/perdido* gene, which is crucial for muscle-tendon attachment (Estrada et al., 2007; Schnorrer et al., 2007) (Figure S4E). In contrast, IFM ablation did not affect bristle orientation in control or *fz* mutant flies, consistent with the lack of an obvious effect on tissue flow orientation (Figures 3Av, 3Av', 3Avii, and 3Avii'). Taken together, these results strongly suggested that tissue flow might be the mechanism responsible for core group-independent PCP in the *Drosophila* notum, and that this flow orients the bristles in the opposing direction.

Loss of *ds* has little influence on notum bristle polarity or tissue flow

The Dachsous (Ds)-Fat (Ft) group consists of the atypical cadherins Ds and Ft and the Golgi kinase Four-jointed (Blair and McNeill, 2018). Although the Ds-Ft group provides global directional cues to regulate the orientation of core group protein asymmetry in several *Drosophila* tissues (Ma et al., 2003; Yang et al., 2002), in the abdomen, the Ds-Ft group and the core group are known to act independently to regulate PCP (Casal et al., 2006). However, we found that loss or RNAi knockdown of any one of several Ds-Ft group genes did not affect the reversed notum bristle orientation in *chas*, *stbm* RNAi flies (Figure 4A; data not shown). Moreover, loss of *ds* had little influence on the angle or velocity of tissue flow compared with controls (Figures 4B–4D). These data suggested that the Ds-Ft group is not involved in regulating tissue flow-induced notum bristle polarity.

Mechanical events that place a bristle cell in the correct position

To determine how tissue flow orients bristles in the opposite direction independently of the core group, we re-analyzed our time-lapse movies of cell flow in control, *fz* mutant, and *stbm* RNAi nota (Videos S3 and S4), focusing on the ES organs (Figure 5A). In controls at 26 hAPF, before bristle cell sprouting, the bristle cell was already enveloped by its paired socket cell and positioned on its anterior side (Figures 5B–5D). During 28–34 hAPF, the extending bristle cell became more precisely aligned along the anterior-posterior axis (Figures 5B–5D). In contrast, at 26 hAPF in *fz* mutant and *stbm* RNAi pupae, the bristle cell of a pair was randomly located at the periphery of the socket cell. Furthermore, as the bristle developed, it shifted toward the anterior side of the socket cell (Figures 5B–5D; Videos S3 and S4). By 30–32 hAPF, the bristle cell had adopted a biased localization on the anterior side of the socket cell, similar to the near-normal bristle orientation in *stbm* RNAi pupae (Figure 1D; Video S2).

We speculated that this repositioning of the bristle cells in *fz* mutant and *stbm* RNAi pupae might reflect a simple physical phenomenon, such as apical extracellular substances functioning as a physical barrier to restrict bristle tip movement. Only when bristles sprouted in an abnormal direction would this restriction cooperate with cell flow and cause the bristles to orient in the direction opposite to that of the tissue flow. Our hypothesis is supported by the following observations. First, the socket cells enveloping bristle cells communicate mainly with neighboring epithelial cells (Figure 2B). Although it is theoretically possible that socket cells might be involved in bristle cell repositioning, when we knocked down the *bazooka* (*baz*) gene in control and *chas*, *stbm* RNAi pupae to eliminate socket cells (Bellaiche and Schweisguth, 2001; Betschinger and Knoblich, 2004; Mummery-Widmer et al., 2009), we saw no differences in effects on bristle polarity phenotype (Figures S5A–S5C, S5B', and S5C'). This finding indicates that the socket cell is not necessary for cell flow-induced regulation of bristle polarity. We also found that, in the *fz* mutant or *chas*, *stbm* RNAi backgrounds, bristle orientation sometimes changed toward the direction opposite to that of the tissue flow without a change in cell body position (Figure S5D). In this situation, epithelial cells surrounding the socket cells also did not move along the periphery of the socket cell (Figure S5D), suggesting no direct involvement of the surrounding epithelial cells in bristle reorientation.

The second observation supporting our hypothesis is that, when a core group gene was inactivated, the position of the bristle cells moved clockwise (CW) or counter-clockwise (CCW) along the periphery of the socket cell on the left half of the notum (Figures 6A and 6B). This choice of CW or CCW movement depended on the initial position of the bristle cell relative to its destination position (in this case, the anterior side of the socket cell), and took the shortest route (Figure 6C). This outcome appears to reflect a simple physical interaction

Figure 4. Loss of *ds* has little influence on either flow-mediated bristle polarity control or normal tissue flow in the notum

(A) (i and ii) Macroscopic dorsal views of the nota of adult (i) *ds* mutant ($ds^{-/-}$) flies and (ii) $ds^{-/-}$ flies in which *chas* and *stbm* were knocked down by RNAi ($ds^{-/-}$ *chas*, *stbm* RNAi). (i' and ii') Rose diagrams showing the angular distribution of the bristles in the A regions of the nota in (i and ii).

(B) Trajectories of socket cells in the A region of E-cadherin::GFP-labeled notum epithelium in (i) control and (ii) $ds^{-/-}$ pupae. Left panels, the position of socket cells at 24 hAPF; middle panels, trajectories of socket cells during 24–28 hAPF; right panels, trajectories of socket cells during 24–34 hAPF. *aDC macrochaetae. Scale bar, 20 μm.

(C) Quantification of the results in (B). Rose diagrams show the angles of the movements of socket cells during each indicated 2 h window in (i) control and (ii) $ds^{-/-}$ pupae. Angles were measured between consecutive frames of each time-lapse series at 10 min intervals.

(D) Quantitation of tissue flow velocity data for (B). Results are the mean velocity of the tissue flow (socket cells) during each 2 h window in (i) control and (ii) $ds^{-/-}$ pupae. Data are the mean ± SD. ***$p < 0.005$, ****$p < 0.0001$ by Mann-Whitney test.

CellPress
OPEN ACCESS

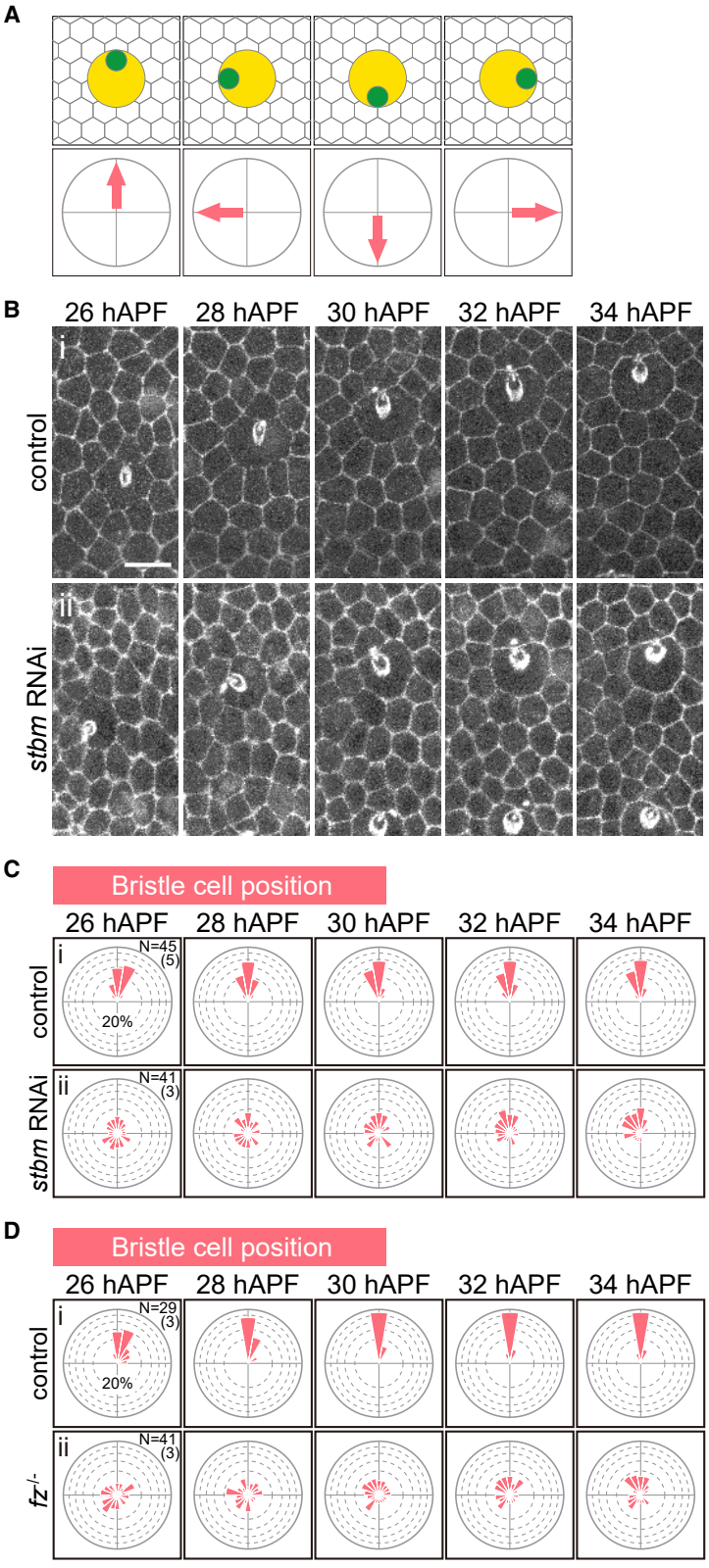

Figure 5. The mislocalization of bristle cells in ES organs depleted of a PCP core group gene is rescued by tissue flow

(A) Top: schematic diagrams of the dorsal views of bristle (green)-socket (yellow) pairs with normal (the leftmost panel) and abnormal (the remaining three panels) bristle cell position. In each case, the bristle-socket pair is surrounded by epithelial cells. Bottom: schematic representations indicating the position of the bristle cell in the ES organ in the top panels.

(B) Time-lapse live imaging over the indicated time periods of bristle-socket pairs in the A region of E-cadherin::GFP-labeled notum epithelium in (i) *pnr*-Gal4 (control) and (ii) *pnr*-Gal4>UAS-*stbm*-IR (*stbm* RNAi) pupae. Images are derived from the time-lapse imaging experiments in Figure S2E. Scale bar, 10 μm.

(C) Quantification of the results in (B). Rose diagrams showing the position of the bristle cell in the ES organ at the indicated times in (i) control and (ii) *stbm* RNAi pupae. The same time-lapse imaging data as in Figure S2E were used to generate these results, but we used a "bristle cell position" analysis that was not performed in Figures S2 and S3.

(D) Quantification of the results in Figure 2C. Rose diagrams showing the position of the bristle cell in the ES organ at the indicated times in the (i) control and (ii) $fz^{-/-}$ pupae. The same time-lapse imaging data as in Figure 2C were used to generate these results, but we used a different quantitative analysis that was not performed in Figure 2. See also Videos S3 and S4.

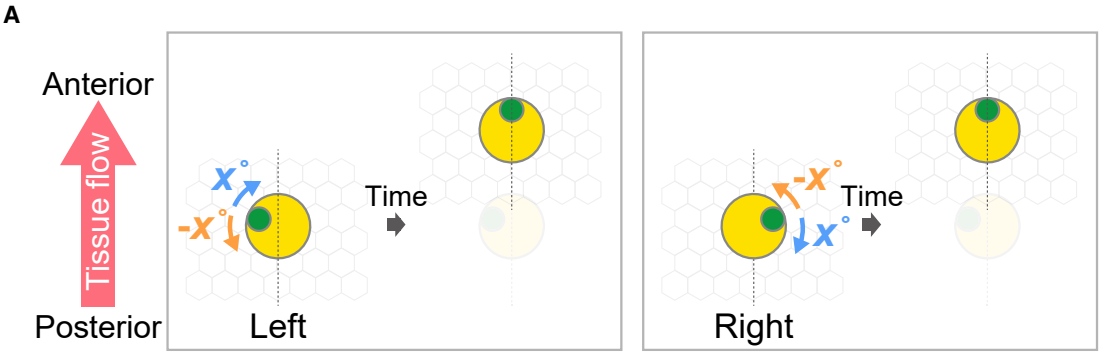

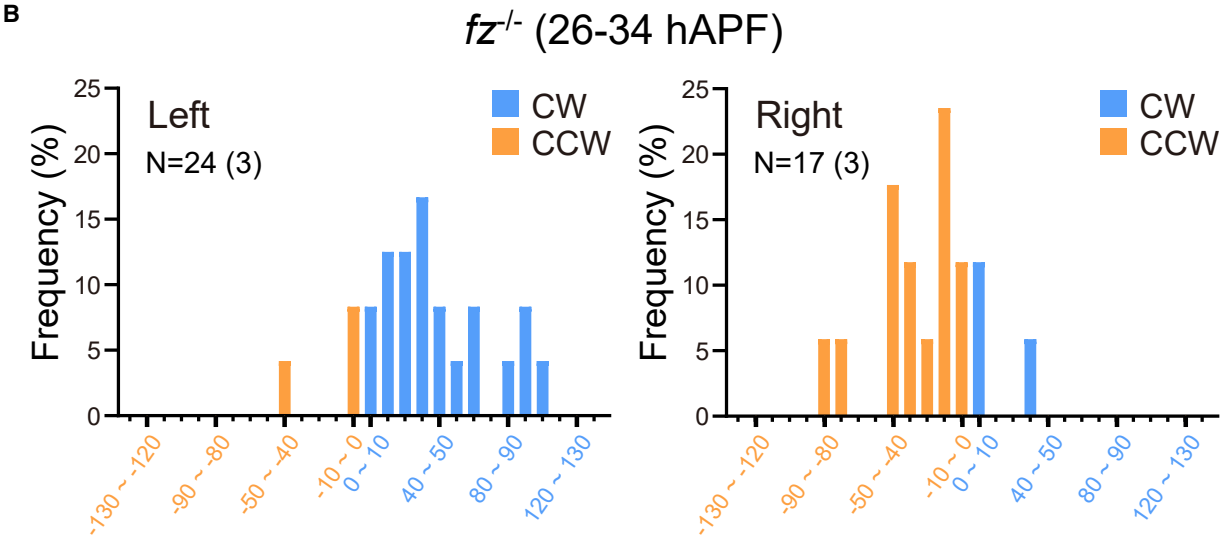

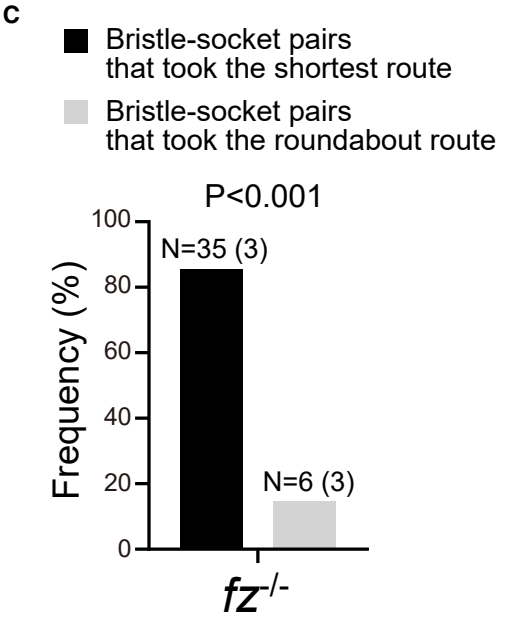

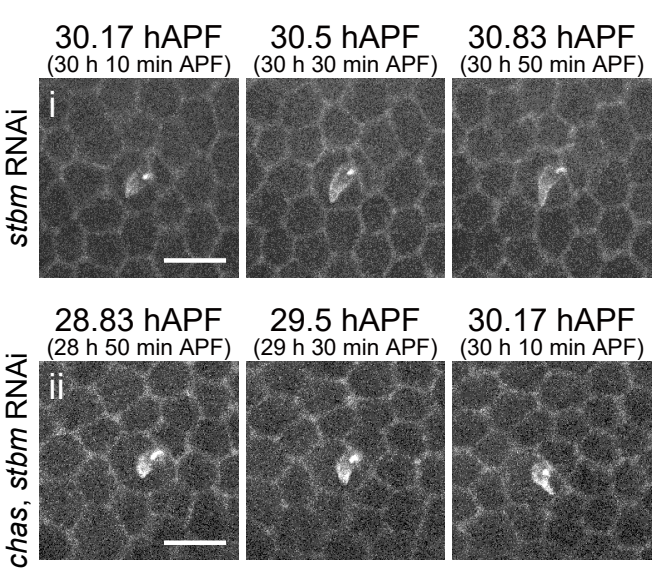

(legend on next page)

(e.g., friction) between the bristles and apical extracellular substances, consistent with the curving of bristle shafts during repositioning (Figure 6D). Collectively, these data suggested that there is a physical association between bristles and apical extracellular substances that affects PCP.

aECM lies in close proximity to bristle tips and hardly moves during tissue flow

To dissect the involvement of apical extracellular substances in bristle cell repositioning, we concentrated on the key apical extracellular matrix (aECM) component Dumpy (Dpy), which anchors epidermal cells to the pupal cuticle to define tissue shape (Chu and Hayashi, 2021; Muller et al., 2013; Wilkin et al., 2000). We live imaged the nota of control and *chas*, *stbm* RNAi pupae using a protein trap line expressing Dpy::YFP under the control of the endogenous promoter (Lowe et al., 2014; Lye et al., 2014), and the sChMCA line, which expresses the mCherry-tagged actin-binding domain of Moesin (Abreu-Blanco et al., 2011). In both control and *chas*, *stbm* RNAi nota, the bristle tips were in close proximity to Dpy during the bristle-sprouting stage (28 hAPF) (Figure 7A), suggesting that bristles can make contact with Dpy in the aECM during repositioning.

If aECM is acting as the factor utilized by tissue flow to orient bristles in the opposite direction, aECM should not move together with the underlying epithelium. To test this notion, we performed time-lapse live imaging of pupae expressing Dpy::YFP and sChMCA. During pupal development, the Dpy matrix exhibits complex 3D structures that change dynamically in response to mechanical tension (Chu and Hayashi, 2021), making it difficult to follow matrix behavior. Therefore, we photobleached a small area within the Dpy::YFP-positive extracellular region to serve as a landmark for tracking Dpy matrix movement. In control and *stbm* RNAi nota, while the epithelial cells flowed anteriorly, the Dpy matrix moved slightly in the direction opposite to that of the tissue flow (Figures S6Ai, S6Aii, S6Aiv, S6Av, S6Avii, and S6Aviii). In *chas*, *stbm* RNAi nota, the epithelial cells flowed posteriorly, whereas the Dpy matrix barely moved (Figures S6Aiii, S6Avi, and S6Aix). These results implied that aECM does not move together with the epithelium and so is a promising candidate for the extracellular factor required for bristle polarity regulation.

In our photobleaching experiments, recovery of Dpy::YFP fluorescence was observed in regions with underlying epithelial cells (Figures S6Ai, S6Aii, and S6Aiii), confirming a previous result showing that notal epithelial cells (tendon cells) produce and secrete Dpy (Chu and Hayashi, 2021). Consistent with this finding, knockdown of *dpy* specifically in ES organs (by using *neuralized*-Gal4) did not affect either the Dpy::YFP distribution pattern or adult bristle orientation (data not shown). Thus, notal epithelial cells appear to play a crucial role in establishing the Dpy distribution pattern.

Dpy knockdown decreases changes in bristle orientation

We next tested whether decreasing Dpy expression affected the regulation of bristle polarity induced by tissue flow. Depletion of *dpy* is known to attenuate the attachment between epidermal cells and the pupal cuticle, making the notum epithelium susceptible to IFM mechanical pulling force (Chu and Hayashi, 2021; Wilkin et al., 2000). When *dpy* was knocked down in wild-type nota, the orientation of the tissue flow was reversed by IFM mechanical pulling force (data not shown). To circumvent this obstacle, we used *chas*, *stbm* RNAi pupae as controls and compared them with pupae in which *dpy* was also knocked down (*dpy*, *chas*, *stbm* RNAi pupae). In *chas*, *stbm* RNAi pupae, the epithelial tissue moved in the reverse (posterior) direction in response to IFM pulling (as occurred in *dpy*-depleted wild-type pupae) (Video S4). However, in *dpy*, *chas*, *stbm* RNAi pupae (but not control *chas*, *stbm* RNAi pupae), pronounced epidermal indentations appeared in the A region at 30–31 hAPF (data not shown), making it difficult to track the developing bristles after this stage in live imaging studies. Therefore, we confined our analyses to the 28–31 hAPF period. In control *chas*, *stbm* RNAi pupae at the start of bristle formation, the bristles pointed in various directions before undergoing a repositioning at 28–31 hAPF that caused them to become oriented in the direction opposite to that of the reversed tissue flow (Figures 7Bi, 7Ci, 7Di, S6B, and S6C). Importantly, depletion of *dpy* in *chas*, *stbm* RNAi pupae significantly reduced these changes to tissue flow-induced bristle orientation (Figure S6D) and inhibited a reversal of bristle orientation (Figures 7Bii, 7Cii, and 7Dii), despite the fact that *dpy* depletion made the angle of the reversed flow more posterior and accelerated the velocity of the cell flow in the epithelium compared with *chas*, *stbm* RNAi controls (Figures S7A–S7C).

We noted a difference in bristle orientation between *chas*, *stbm* RNAi pupae and *dpy*, *chas*, *stbm* RNAi pupae at 28 hAPF (Figure 7C) that prompted us to compare the positions of bristle cells in *chas*, *stbm* RNAi and *dpy*, *chas*, *stbm* RNAi ES organs

Figure 6. The positions of bristle cells in an ES organ depleted of a PCP core group gene move clockwise or counter-clockwise to reach their destination by the shortest route

(A) Left panel: normal tissue flow orientation from posterior to anterior. Middle and right panels: schematic diagrams of two types of bristle-socket pairs with abnormal bristle cell orientation. Middle: the bristle cell's position slants to the left relative to the anterior-posterior axis and may move clockwise (CW) or counter-clockwise (CCW). Right: the bristle cell's position slants to the right relative to the anterior-posterior axis, and may also move CW or CCW. Green, bristle cell; yellow, socket cell.

(B) Quantitation of the time-lapse imaging data in Figure 2C. Results are the percent frequency of CW or CCW movement of the indicated angle x° in the ranges shown on the x axis for ES organs with the left-slanting and right-slanting bristle cells in $fz^{-/-}$ pupae during 26–34 hAPF.

(C) Statistical analysis by Fisher's exact test of the results in (B); i.e., the proportions of bristle-socket pairs that took either the shortest route (black), or the roundabout route (gray), in $fz^{-/-}$ pupae during 26–34 hAPF.

(D) Time-lapse live imaging at the indicated times of developing bristles labeled with sGMCA in the A region of (i) *stbm* RNAi and (ii) *chas*, *stbm* RNAi nota. Note that the bristles were often curved during the repositioning of the bristle cells. The images in Figure 6Di were derived from the time-lapse imaging experiments in Figure 1C. The bristle-socket pair in Figure 6Dii is identical with that in Figure S5Dii. Scale bars, 10 μm.

See also Figure S5 and Video S3.

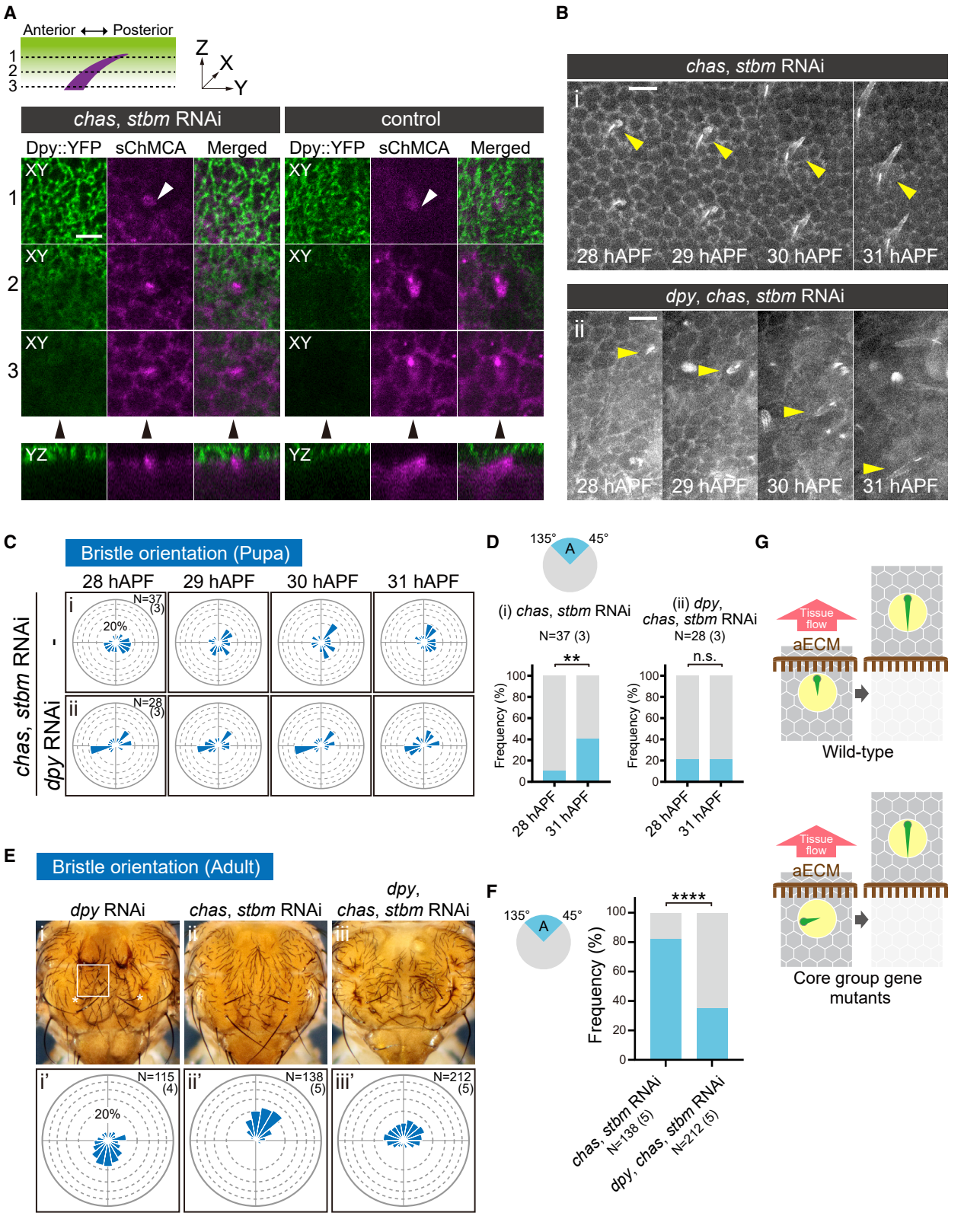

(legend on next page)

before the onset of bristle formation. We found that the bristle cells were positioned near randomly at 26 hAPF in both strains. In fact, the position of *dpy*, *chas*, *stbm* RNAi bristle cells was slightly biased toward the lateral and medial directions (Figure S7D), perhaps accounting for the difference in bristle orientation observed at 28 hAPF. Furthermore, unlike adult *chas*, *stbm* RNAi flies, adult *dpy*, *chas*, *stbm* RNAi flies showed a reduced degree of PCP reversal, with anteriorly biased randomness in bristle orientation (Figures 7E and 7F), bolstering our data showing that *dpy* knockdown decreases changes in bristle orientation. Consistent with these findings, bristles in adult *dpy* RNAi flies were still oriented in a posteriorly biased manner (Figure 7Ei), despite the fact that *dpy* RNAi pupae exhibited a reversed tissue flow with increased velocity (compared with *chas*, *stbm* RNAi pupae) (data not shown). Taken together, these data demonstrate that the aECM serves as a physical barrier that cooperates with tissue flow to align notum bristles in the opposite direction.

PCP regulation by tissue flow can explain the bristle orientation defect in *dpy* mutants

Our proposed mechanism is shown in Figure 7G. While most of the data presented above support our model, the fact that *dpy* mutants exhibit abnormal bristle orientation around indentations in the notum epithelium (Carmon et al., 2010; Chu and Hayashi, 2021; Metcalfe, 1970; Muller et al., 2013; Olguin et al., 2011; Wilkin et al., 2000) seems to be contradictory. In our model, the ability of Dpy to act as a physical barrier influencing bristle alignment should be attenuated in *dpy* mutants, so that bristle orientation defects should not obviously appear around indentations even when cell flow direction is perturbed by mechanical pulling force near the indentation. We hypothesized that this discrepancy might be explained by the degree of loss of *dpy* function. We knocked down *dpy* to varying degrees in *stbm* RNAi flies by using two different *dpy* RNAi lines and changing the rearing temperature (the Gal4/UAS system is temperature-dependent), and examined effects on notal phenotypes. The difference in the knockdown effect on *dpy* in these two RNAi lines was confirmed by examination of notum phenotypes and Dpy::YFP expression (Figure S7E; data not shown). A combination of *stbm* knockdown plus strong *dpy* knockdown resulted in randomized bristle orientation with notum malformation (Figures S7Fi and S7Fi'). In contrast, *stbm* knockdown plus weak *dpy* knockdown led to a reversal of bristle orientation with notum malformation (Figures S7Fii and S7Fii'). Live imaging experiments showed that the tissue flow orientation was reversed in both strains (data not shown). Thus, weak *dpy* knockdown substantially diminished the ability of the notum to resist external forces but still allowed aECM to act as a physical barrier aligning bristles. This phenotype is similar to that of *dpy* mutants, where the bristle orientation around epithelial indentations is affected (Chu and Hayashi, 2021; Metcalfe, 1970; Muller et al., 2013; Olguin et al., 2011; Wilkin et al., 2000).

The validity of our model is also supported by the phenotype of flies with double loss of function of *dpy* plus *chas*. In double mutants of hypomorphic *dpy* allele with a *chas* null allele, indentations were observed in the notum lateral region (just outside the A region), which is near the DVM attachment site (Figures S4D and S7Gii). The bristle orientation defect (away from the indentations and toward the midline) was most obvious in the A region (Figures S7Gii and S7Gii') (Olguin et al., 2011). Both the indentation and bristle abnormalities in *chas*, *dpy* double mutants were completely suppressed by IFM ablation (data not shown). Compared with *chas*, *dpy* mutants, a combination of *chas* knockdown plus strong *dpy* knockdown showed more obvious indentations in the lateral region but bristles in the A region were not oriented toward the midline (Figures S7Giii and S7Giii'). On the other hand, *chas* knockdown plus weak *dpy* knockdown exhibited a milder notum phenotype. There were no obvious indentations in the lateral region but a stronger bristle phenotype appeared in the A region (like *chas*, *dpy* mutants), with the bristles oriented toward the midline (Figures S7Giv and S7Giv'). These results suggested that enhanced mechanical disruption of the notum due to *dpy* depletion does not necessarily exacerbate the bristle orientation phenotype. Taken together, we conclude that our model remains a viable explanation for the bristle orientation defect in *dpy* mutants.

DISCUSSION

Based on our study of the *Drosophila* notum, we propose that tissue flow can mediate core group-independent PCP, and that

Figure 7. aECM cooperates with tissue flow to align bristles in the opposite direction

(A) Top: schematic diagram of a developing bristle of a wild-type notum showing the anterior and posterior directions and three focal planes: (1) tip of the bristle; (2) middle of the bristle shaft; and (3) bottom of the bristle shaft. Bottom: fluorescence imaging of the dorsal (xy plane) and orthogonal (yz plane) views of the A region at 28 hAPF of the notum of a live *chas*, *stbm* double RNAi pupa and a control pupa. Crossing to transgenic lines *dpy*::YFP and sChMCA was performed to visualize aECM Dpy (green) plus the bristles and the neighboring epithelial cells (magenta), respectively. White arrowhead, tip of the developing bristle. Black arrowheads, positions of yz planes. Scale bar, 5 μm.

(B) Time-lapse live imaging of bristles labeled with sGMCA in the A region of nota of (i) *chas*, *stbm* double RNAi pupae and (ii) *dpy*, *chas*, *stbm* triple RNAi pupae. Yellow arrowheads, an individual bristle of the same ES organ is shown at the indicated times. Scale bars, 10 μm.

(C) Quantification of the results in (B). Rose diagrams showing the angular distribution of the bristles in (i) *chas*, *stbm* double RNAi pupae and (ii) *dpy*, *chas*, *stbm* triple RNAi pupae at the indicated times.

(D) The proportion of bristles pointing to either the anterior direction (A) or to any other direction are indicated in blue and gray, respectively, in (i) *chas*, *stbm* RNAi pupae and (ii) *dpy*, *chas*, *stbm* RNAi pupae at the indicated times. **$p < 0.01$ by Fisher's exact test.

(E) Macroscopic dorsal views of bristle phenotypes in the A region (white box) of the nota of adult (i) *dpy* RNAi, (ii) *chas*, *stbm* RNAi, and (iii) *dpy*, *chas*, *stbm* RNAi flies. *aDC bristle. (i'–iii') Rose diagrams showing the angular distribution of the bristles in the A regions of the flies in (i–iii).

(F) The proportion of bristles pointing to either the anterior direction (A) or to any other direction are indicated in blue and gray, respectively, in *chas*, *stbm* RNAi and *dpy*, *chas*, *stbm* RNAi flies. ****$p < 0.0001$ by Fisher's exact test.

(G) Schematic diagram of the "flow and comb" model. See main text for details.

See also Figures S6 and S7.

mechanical events arising from interactions between tissue flow and aECM can align bristles. In our model, tissue flow acts like a "hairdresser" that uses an aECM "comb" to orient bristles in the direction opposite to that of the tissue flow (Figure 7G). Although we cannot completely rule out other possibilities, our "flow and comb" model is strongly supported by the following experimental results (1) bristles change their orientation in response to tissue flow manipulation (Figures 3, S1, S2, and S3); (2) bristle cells behave as they might be expected to if they were responding to friction during tissue flow (Figure 6); and (3) bristle orientation changes are inhibited by knockdown of an aECM component (Figures 7 and S6D). Our study therefore exposes a unique aspect of PCP regulation by demonstrating the significance of cooperation between tissue dynamics and extracellular substances.

Tissue flow was originally reported as being involved in reorientation of core protein asymmetry and proper PCP formation in the *Drosophila* wing (Aigouy et al., 2010; Merkel et al., 2014). In our study, we have shown that tissue flow plays a crucial role in PCP formation on the notum, as represented by the regulation of bristle orientation, and that this effect is independent of core group function. Our results offer a broadened view of the roles of collective cell behavior in PCP regulation.

During early pupal development (27–28 hAPF) of wild-type flies, as newly formed ES organs with the bristle cell positioned on the anterior side of the socket cell move anteriorly together with notal epithelial cells, the bristle cell starts to sprout in the posterior direction and then elongates posteriorly. On the other hand, in a pupal notum depleted of PCP core group function, the configuration of the cells in the ES organ before the bristle starts to sprout differs from that in the wild type. Rather than being positioned on the anterior side of the socket cell, the bristle cell is randomly located at its periphery (Figures 5Bii, 5Cii, and 5Dii). This abnormality probably results from the random spindle orientation in SOP cells caused by loss of core group function (Bellaiche et al., 2001; Gho and Schweisguth, 1998; Lu et al., 1999). The randomly located bristle cell then starts to sprout in any direction, but since notal epithelial cells flow anteriorly, the physical association between the bristle and the aECM changes the bristle orientation to the posterior. As a result, the bristle cell position improves and bristle polarity becomes near-normal (Figures 1Cii, 1Dii, 5Bii, 5Cii, and 5Dii). In *chas*, *fz* mutants (or *chas*, *stbm* RNAi flies), where the orientation of bristles is reversed compared with the wild-type controls, tissue flow direction is reversed, and manipulating this flow from the reverse direction to the normal direction suppresses a reversal of bristle orientation (Figures 3, S1, S2, and S3). These results, combined with other data in this study, imply that tissue flow can orient bristles in the opposite direction. Importantly, this flow-mediated mechanism seems to function not only when the core group system is impaired but also in intact flies. Even in wild-type control pupae, the position of the bristle cell in the ES organ becomes more precisely aligned along the anterior-posterior axis during normal tissue flow (Figures 5Ci and 5Di), suggesting that the "flow and comb" mechanism is not just a back-up to the core group system.

In this study, we demonstrated that the bristle tips lie in close proximity to aECM Dpy, and that *dpy* RNAi decreases tissue flow-mediated changes in bristle orientation in *chas*, *stbm* RNAi flies (Figures 7, S6, and S7). These data suggest that Dpy helps to establish and rectify PCP by forming the comb to align bristles. Importantly, the validity of this aECM comb-mediated mechanism for regulating bristle orientation is also supported by our observation that the bristles of some ES organs with abnormal cellular configuration become oriented in the opposite direction to that of tissue flow without changing the position of the bristle cells (Figure S5D).

Although previous results showing that *dpy* mutants exhibit abnormal bristle orientation in the notum epithelium (Carmon et al., 2010; Chu and Hayashi, 2021; Metcalfe, 1970; Muller et al., 2013; Olguin et al., 2011; Wilkin et al., 2000) seem to conflict with our proposed model (Figure 7G), we demonstrated that this discrepancy can be explained (at least in part) by the degree of loss of *dpy* function (Figures S7E–S7G). However, this may not be the whole story behind how *dpy* loss contributes to bristle orientation abnormalities. Consistent with our proposed model, despite a reversal of notal tissue flow with increased velocity in *dpy* RNAi pupae (data not shown), bristles in adult *dpy* RNAi flies still exhibit posteriorly biased orientation but with weak randomness (Figures 7Ei and 7Ei'). How can this weak randomness be explained? It may be that, in *dpy* RNAi pupae, although the aECM comb effect is significantly reduced compared with that in wild-type or weak *dpy* RNAi pupae, residual comb activity remains (albeit very slight). Indeed, we showed that *dpy* RNAi significantly decreases changes in bristle orientation via tissue flow (Figures 7B–7D and S6D), but that this suppression effect is not complete. Therefore, this weak randomness of bristle orientation in adult *dpy* RNAi flies may be due to a combination of the residual very weak comb effect and the reversed tissue flow, and may partially reflect the process by which a bristle slowly changes its orientation from the normal (posterior) to the opposite (anterior) direction. Other aECM components may be involved in comb formation to contribute this weak phenotype. Another potential explanation for this weak phenotype might be that the global orientation of the epithelial sheet is disrupted or distorted by the abnormal traction of the epithelium through the IFMs. Finally, because we found that the positions of bristle cells before the onset of bristle formation differed between *chas*, *stbm* RNAi and *dpy*, *chas*, *stbm* RNAi ES organs (Figure S7D), it may be that Dpy is involved in an unknown process that is needed for the arrangement of ES organ cells. Further studies will be needed to fully understand the multifunctional nature of Dpy.

Another area that will require future investigation is the notum's ability to resist external forces. We showed that reversal of tissue flow in the central region of the notum requires the loss of function of not only *chas* but also that of a core group gene (Figures 3A–3C, S1, S2, and S3). Our data indicate that the notum's ability to resist external forces is more impaired in *chas*, *stbm* RNAi pupae (or *chas*, *fz* mutants) than in *chas* RNAi pupae (or *chas* mutants). Thus, the core group proteins may possess a crucial role in resistance to IFM-mediated pulling force.

More work is also necessary to elucidate the mechanism governing normal tissue flow on the notum. Since loss of function of the core group or Ds does not result in severe defects in flow direction or velocity in the central notum (Figures 4B–4D), other

mechanisms must be involved. In the fly abdomen, aECM proteins are important for the collective migration of larval epithelial cells (Bischoff, 2012; Ninov et al., 2010), making it possible that aECM is also required for normal tissue flow in the notum. Although we found that *dpy* knockdown accelerated the velocity of the reversed tissue flow in *chas*, *stbm* RNAi pupae, and that this aberrant flow was driven by IFM-mediated pulling force (Figure S7C), there are likely other ECM components (potentially additional aECM factors and/or basal ECM proteins) involved in regulating this reversed flow. Morphogenetic events in the *Drosophila* notum (including tissue flow) are complex and involve many cellular processes, including cell division, rearrangement, and changes to cell size and shape (Guirao et al., 2015). Our results reflect this complexity since the central and lateral regions of the notum differed greatly in their dependence on the core group for tissue flow formation (Figures S4A–S4C). A previous observation that tissue flow formation does not start simultaneously in all regions of the notum (Bosveld et al., 2012) may be related to this difference in the flow control mechanism for each region of the notum. Future interdisciplinary studies as proposed previously (Guirao et al., 2015) will be necessary to comprehensively dissect notal tissue dynamics.

How do our findings in *Drosophila* relate to tissue dynamics in vertebrates? Motile cilia found in the trachea and brain ventricle exhibit planar beating that results in directional, external fluid flow. This planar polarity of cilia and the directional fluid flow are mutually interdependent: generation of the directional fluid flow requires coordinated beating of the cilia, and the planar polarity of the cilia is regulated by the directional flow in a positive feedback manner (Wallingford, 2010). Although immotile external structures, such as bristles, cannot generate external fluid flow, our work shows that an analogous mechanism that couples tissue flow with aECM regulates bristle orientation on the *Drosophila* notum. These two phenomena resemble each other in that external forces contribute to PCP in both cases. However, these mechanisms differ greatly in their dependence on the core group of PCP proteins. In the mouse brain ventricle, external fluid flow orients motile cilia through the function of the core group protein Vangl2 (the mammalian ortholog of *stbm*) (Guirao et al., 2010), whereas, on the *Drosophila* notum, tissue flow regulates bristle orientation independently of PCP core group function. Is the tissue flow-induced mechanism (or a related process) utilized in mammals and other vertebrates? In the mammalian inner ear, hair cells form directed stereocilia bundles on their apical surfaces, which then attach to aECM (the tectorial membrane) (Goodyear and Richardson, 2018). Intriguingly, it was shown previously that the embryonic PCP defect in the cochlea of Vangl2-deficient mutant mice was rescued by an unknown mechanism during neonatal development (Copley et al., 2013). Thus, a cell flow-induced mechanism (or a similar process) that is independent of PCP core group function may act on mammalian tissues featuring aECM. Future studies will be needed to elucidate if the tissue flow-induced PCP regulatory mechanism highlighted by our study is evolutionarily conserved.

Limitations of the study

Our study proposes a model in which aECM, in addition to its role in modulating the mechanical properties of the notum, functions like a comb to orient bristles in the direction opposite to that of tissue flow. Experiments based on the loss of function of an aECM component were employed to derive this model, but we were not able to perform these assays under conditions where only the comb effect of aECM was deficient. In addition, whether the interaction between a bristle tip and aECM is simply a physical contact or involves a chemical interaction is also unclear at this time. Furthermore, although we found that reversed notal tissue flow is caused by IFM-mediated mechanical pulling force, the mechanism governing normal tissue flow on the notum remains elusive.

STAR★METHODS

Detailed methods are provided in the online version of this paper and include the following:

- KEY RESOURCES TABLE
- RESOURCE AVAILABILITY
  - Lead contact
  - Materials availability
  - Data and code availability
- EXPERIMENTAL MODEL AND SUBJECT DETAILS
  - *Drosophila* strains and genetics
- METHOD DETAILS
  - Live imaging analysis
  - Analysis of time-lapse images
  - Histological analyses
- QUANTIFICATION AND STATISTICAL ANALYSIS

SUPPLEMENTAL INFORMATION

Supplemental information can be found online at https://doi.org/10.1016/j.celrep.2022.111388.

ACKNOWLEDGMENTS

We thank P. Adler, D. Kiehart, U. Nongthomba, S. Artavanis-Tsakonas, the Kyoto Stock Center, the Vienna Drosophila Resource Center (VDRC), the Bloomington Drosophila Stock Center, and the Transgenic RNAi Project (TRiP) for fly stocks; N. Odaka, M. Suzuki, M. Ito, and E. Todo for technical assistance; S. Hayashi, T. Nakazawa, and S. Takasuga for valuable discussions; and E. Kuranaga and M. Sato for technical advice on live imaging. This work was supported by JSPS KAKENHI grant nos. JP16H04791, JP16K14718, and JP25127703; JST, PRESTO grant no. JPMJPR204C, Japan; the Uehara Memorial Foundation; the Takeda Science Foundation; the Tomizawa Jun-ichi & Keiko Fund of the Molecular Biology Society of Japan for Young Scientists; the Yamada Science Foundation; the Ohsumi Frontier Science Foundation; and Nanken-Kyoten, TMDU (to M.Y.). T.A. was supported by JSPS KAKENHI grant no. JP17K07403, the Kao Foundation for Arts and Sciences, the Kato Memorial Bioscience Foundation, and the Uehara Memorial Foundation. M.A. was supported by JSPS KAKENHI grant nos. JP15K20835, JP15H05857, and JP20H05948.

AUTHOR CONTRIBUTIONS

M.Y. and T.A. designed the experiments. T.A. and M.Y. carried out the experiments. M.Y., T.A., and M.A. performed the data analyses. M.A. and K.I. contributed to constructing the hypothesis via theoretical analyses. Y.H., J.S., H.S., and T.S. contributed to the imaging experiments. M.Y. wrote the paper with input from the other authors.

DECLARATION OF INTERESTS

The authors declare no competing interests.

Received: August 24, 2021
Revised: July 16, 2022
Accepted: August 29, 2022
Published: September 20, 2022

REFERENCES

Abreu-Blanco, M.T., Verboon, J.M., and Parkhurst, S.M. (2011). Cell wound repair in *Drosophila* occurs through three distinct phases of membrane and cytoskeletal remodeling. J. Cell Biol. *193*, 455–464.

Adler, P.N., Charlton, J., and Vinson, C. (1987). Allelic variation at the *frizzled* locus of *Drosophila*. Dev. Genet. *8*, 99–119.

Adler, P.N., Charlton, J., and Liu, J. (1998). Mutations in the cadherin superfamily member gene *dachsous* cause a tissue polarity phenotype by altering *frizzled* signaling. Development *125*, 959–968.

Adler, P.N. (2002). Planar signaling and morphogenesis in *Drosophila*. Dev. Cell *2*, 525–535.

Aigouy, B., Farhadifar, R., Staple, D.B., Sagner, A., Röper, J.C., Jülicher, F., and Eaton, S. (2010). Cell flow reorients the axis of planar polarity in the wing epithelium of *Drosophila*. Cell *142*, 773–786.

Amonlirdviman, K., Khare, N.A., Tree, D.R.P., Chen, W.S., Axelrod, J.D., and Tomlin, C.J. (2005). Mathematical modeling of planar cell polarity to understand domineering nonautonomy. Science *307*, 423–426.

Axelrod, J.D. (2001). Unipolar membrane association of Dishevelled mediates Frizzled planar cell polarity signaling. Genes Dev. *15*, 1182–1187.

Axelrod, J.D. (2020). Planar cell polarity signaling in the development of left-right asymmetry. Curr. Opin. Cell Biol. *62*, 61–69.

Ayukawa, T., Akiyama, M., Mummery-Widmer, J.L., Stoeger, T., Sasaki, J., Knoblich, J.A., Senoo, H., Sasaki, T., and Yamazaki, M. (2014). Dachsous-dependent asymmetric localization of spiny-legs determines planar cell polarity orientation in *Drosophila*. Cell Rep. *8*, 610–621.

Bastock, R., Strutt, H., and Strutt, D. (2003). Strabismus is asymmetrically localised and binds to Prickle and Dishevelled during *Drosophila* planar polarity patterning. Development *130*, 3007–3014.

Bellaïche, Y., Gho, M., Kaltschmidt, J.A., Brand, A.H., and Schweisguth, F. (2001). Frizzled regulates localization of cell-fate determinants and mitotic spindle rotation during asymmetric cell division. Nat. Cell Biol. *3*, 50–57.

Bellaïche, Y., and Schweisguth, F. (2001). Lineage diversity in the *Drosophila* nervous system. Curr. Opin. Genet. Dev. *11*, 418–423.

Betschinger, J., and Knoblich, J.A. (2004). Dare to be different: asymmetric cell division in *Drosophila*, *C. elegans* and vertebrates. Curr. Biol. *14*, R674–R685.

Blair, S., and McNeill, H. (2018). Big roles for Fat cadherins. Curr. Opin. Cell Biol. *51*, 73–80.

Bischoff, M. (2012). Lamellipodia-based migrations of larval epithelial cells are required for normal closure of the adult epidermis of *Drosophila*. Dev. Biol. *363*, 179–190.

Bosveld, F., Bonnet, I., Guirao, B., Tlili, S., Wang, Z., Petitalot, A., Marchand, R., Bardet, P.L., Marcq, P., Graner, F., and Bellaïche, Y. (2012). Mechanical control of morphogenesis by Fat/Dachsous/Four-jointed planar cell polarity pathway. Science *336*, 724–727.

Brand, A.H., and Perrimon, N. (1993). Targeted gene expression as a means of altering cell fates and generating dominant phenotypes. Development *118*, 401–415.

Butler, M.T., and Wallingford, J.B. (2017). Planar cell polarity in development and disease. Nat. Rev. Mol. Cell Biol. *18*, 375–388.

Carmon, A., Guertin, M.J., Grushko, O., Marshall, B., and MacIntyre, R. (2010). A molecular analysis of mutations at the complex *dumpy* locus in *Drosophila melanogaster*. PLoS One *5*, e12319.

Casal, J., Lawrence, P.A., and Struhl, G. (2006). Two separate molecular systems, Dachsous/Fat and Starry night/Frizzled, act independently to confer planar cell polarity. Development *133*, 4561–4572.

Cetera, M., Leybova, L., Woo, F.W., Deans, M., and Devenport, D. (2017). Planar cell polarity-dependent and independent functions in the emergence of tissue-scale hair follicle patterns. Dev. Biol. *428*, 188–203.

Chae, J., Kim, M.J., Goo, J.H., Collier, S., Gubb, D., Charlton, J., Adler, P.N., and Park, W.J. (1999). The *Drosophila* tissue polarity gene *starry night* encodes a member of the protocadherin family. Development *126*, 5421–5429.

Chen, W.S., Antic, D., Matis, M., Logan, C.Y., Povelones, M., Anderson, G.A., Nusse, R., and Axelrod, J.D. (2008). Asymmetric homotypic interactions of the atypical cadherin flamingo mediate intercellular polarity signaling. Cell *133*, 1093–1105.

Chu, W.C., and Hayashi, S. (2021). Mechano-chemical enforcement of tendon apical ECM into nano-filaments during *Drosophila* flight muscle development. Curr. Biol. *31*, 1366–1378.e7.

Clark, H.F., Brentrup, D., Schneitz, K., Bieber, A., Goodman, C., and Noll, M. (1995). *Dachsous* encodes a member of the cadherin superfamily that controls imaginal disc morphogenesis in *Drosophila*. Genes Dev. *9*, 1530–1542.

Copley, C.O., Duncan, J.S., Liu, C., Cheng, H., and Deans, M.R. (2013). Postnatal refinement of auditory hair cell planar polarity deficits occurs in the absence of Vangl2. J. Neurosci. *33*, 14001–14016.

Das, G., Jenny, A., Klein, T.J., Eaton, S., and Mlodzik, M. (2004). Diego interacts with Prickle and Strabismus/Van Gogh to localize planar cell polarity complexes. Development *131*, 4467–4476.

Devenport, D. (2014). The cell biology of planar cell polarity. J. Cell Biol. *207*, 171–179.

Donoughe, S., and DiNardo, S. (2011). *Dachsous* and *frizzled* contribute separately to planar polarity in the *Drosophila* ventral epidermis. Development *138*, 2751–2759.

Estrada, B., Gisselbrecht, S.S., and Michelson, A.M. (2007). The transmembrane protein Perdido interacts with Grip and integrins to mediate myotube projection and attachment in the *Drosophila* embryo. Development *134*, 4469–4478.

Feiguin, F., Hannus, M., Mlodzik, M., and Eaton, S. (2001). The ankyrin repeat protein Diego mediates Frizzled-dependent planar polarization. Dev. Cell *1*, 93–101.

Fernandes, J., Bate, M., and Vijayraghavan, K. (1991). Development of the indirect flight muscles of *Drosophila*. Development *113*, 67–77.

Gho, M., and Schweisguth, F. (1998). Frizzled signalling controls orientation of asymmetric sense organ precursor cell divisions in *Drosophila*. Nature *393*, 178–181.

Go, M.J., Eastman, D.S., and Artavanis-Tsakonas, S. (1998). Cell proliferation control by Notch signaling in *Drosophila* development. Development *125*, 2031–2040.

Goodrich, L.V., and Strutt, D. (2011). Principles of planar polarity in animal development. Development *138*, 1877–1892.

Goodyear, R.J., and Richardson, G.P. (2018). Structure, function, and development of the tectorial membrane: an extracellular matrix essential for hearing. Curr. Top. Dev. Biol. *130*, 217–244.

Gubb, D., and García-Bellido, A. (1982). A genetic analysis of the determination of cuticular polarity during development in *Drosophila melanogaster*. J. Embryol. Exp. Morphol. *68*, 37–57.

Gubb, D., Green, C., Huen, D., Coulson, D., Johnson, G., Tree, D., Collier, S., and Roote, J. (1999). The balance between isoforms of the prickle LIM domain protein is critical for planar polarity in *Drosophila* imaginal discs. Genes Dev. *13*, 2315–2327.

Guirao, B., Meunier, A., Mortaud, S., Aguilar, A., Corsi, J.M., Strehl, L., Hirota, Y., Desoeuvre, A., Boutin, C., Han, Y.G., et al. (2010). Coupling between hydrodynamic forces and planar cell polarity orients mammalian motile cilia. Nat. Cell Biol. *12*, 341–350.

Guirao, B., Rigaud, S.U., Bosveld, F., Bailles, A., López-Gay, J., Ishihara, S., Sugimura, K., Graner, F., and Bellaïche, Y. (2015). Unified quantitative characterization of epithelial tissue development. Elife *4*, e08519.

Huang, J., Zhou, W., Dong, W., Watson, A.M., and Hong, Y. (2009). From the Cover: directed, efficient, and versatile modifications of the *Drosophila* genome by genomic engineering. Proc. Natl. Acad. Sci. USA *106*, 8284–8289.

Jenny, A., Darken, R.S., Wilson, P.A., and Mlodzik, M. (2003). Prickle and Strabismus form a functional complex to generate a correct axis during planar cell polarity signaling. EMBO J. *22*, 4409–4420.

Jones, K.H., Liu, J., and Adler, P.N. (1996). Molecular analysis of EMS-induced *frizzled* mutations in *Drosophila melanogaster*. Genetics *142*, 205–215.

Kiehart, D.P., Galbraith, C.G., Edwards, K.A., Rickoll, W.L., and Montague, R.A. (2000). Multiple forces contribute to cell sheet morphogenesis for dorsal closure in *Drosophila*. J. Cell Biol. *149*, 471–490.

Klingensmith, J., Nusse, R., and Perrimon, N. (1994). The *Drosophila* segment polarity gene *dishevelled* encodes a novel protein required for response to the *wingless* signal. Genes Dev. *8*, 118–130.

Koto, A., Kuranaga, E., and Miura, M. (2009). Temporal regulation of *Drosophila* IAP1 determines caspase functions in sensory organ development. J. Cell Biol. *187*, 219–231.

Lawrence, P.A., and Casal, J. (2018). Planar cell polarity: two genetic systems use one mechanism to read gradients. Development *145*, dev168229.

Lowe, N., Rees, J.S., Roote, J., Ryder, E., Armean, I.M., Johnson, G., Drummond, E., Spriggs, H., Drummond, J., Magbanua, J.P., et al. (2014). Analysis of the expression patterns, subcellular localisations and interaction partners of *Drosophila* proteins using a *pigP* protein trap library. Development *141*, 3994–4005.

Lu, B., Usui, T., Uemura, T., Jan, L., and Jan, Y.N. (1999). Flamingo controls the planar polarity of sensory bristles and asymmetric division of sensory organ precursors in *Drosophila*. Curr. Biol. *9*, 1247–1250.

Lye, C.M., Naylor, H.W., and Sanson, B. (2014). Subcellular localisations of the CPTI collection of YFP-tagged proteins in *Drosophila* embryos. Development *141*, 4006–4017.

Ma, D., Yang, C.H., McNeill, H., Simon, M.A., and Axelrod, J.D. (2003). Fidelity in planar cell polarity signalling. Nature *421*, 543–547.

Mauri, F., Reichardt, I., Mummery-Widmer, J.L., Yamazaki, M., and Knoblich, J.A. (2014). The conserved discs-large binding partner Banderuola regulates asymmetric cell division in *Drosophila*. Curr. Biol. *24*, 1811–1825.

McNeill, H. (2010). Planar cell polarity: keeping hairs straight is not so simple. Cold Spring Harbor Perspect. Biol. *2*, a003376.

Merkel, M., Sagner, A., Gruber, F.S., Etournay, R., Blasse, C., Myers, E., Eaton, S., and Jülicher, F. (2014). The balance of prickle/spiny-legs isoforms controls the amount of coupling between core and fat PCP systems. Curr. Biol. *24*, 2111–2123.

Metcalfe, J.A. (1970). Developmental genetics of thoracic abnormalities of dumpy mutants of *Drosophila melanogaster*. Genetics *65*, 627–654.

Müller, R., Jenny, A., and Stanley, P. (2013). The EGF repeat-specific O-GlcNAc-transferase Eogt interacts with notch signaling and pyrimidine metabolism pathways in *Drosophila*. PLoS One *8*, e62835.

Mummery-Widmer, J.L., Yamazaki, M., Stoeger, T., Novatchkova, M., Bhalerao, S., Chen, D., Dietzl, G., Dickson, B.J., and Knoblich, J.A. (2009). Genome-wide analysis of Notch signalling in *Drosophila* by transgenic RNAi. Nature *458*, 987–992.

Ninov, N., Menezes-Cabral, S., Prat-Rojo, C., Manjón, C., Weiss, A., Pyrowolakis, G., Affolter, M., and Martín-Blanco, E. (2010). Dpp signaling directs cell motility and invasiveness during epithelial morphogenesis. Curr. Biol. *20*, 513–520.

Olguín, P., Glavic, A., and Mlodzik, M. (2011). Intertissue mechanical stress affects Frizzled-mediated planar cell polarity in the *Drosophila* notum epidermis. Curr. Biol. *21*, 236–242.

Parks, A.L., Cook, K.R., Belvin, M., Dompe, N.A., Fawcett, R., Huppert, K., Tan, L.R., Winter, C.G., Bogart, K.P., Deal, J.E., et al. (2004). Systematic generation of high-resolution deletion coverage of the *Drosophila melanogaster* genome. Nat. Genet. *36*, 288–292.

Roy, S., and VijayRaghavan, K. (1997). Homeotic genes and the regulation of myoblast migration, fusion, and fibre-specific gene expression during adult myogenesis in *Drosophila*. Development *124*, 3333–3341.

Schindelin, J., Arganda-Carreras, I., Frise, E., Kaynig, V., Longair, M., Pietzsch, T., Preibisch, S., Rueden, C., Saalfeld, S., Schmid, B., et al. (2012). Fiji: an open-source platform for biological-image analysis. Nat. Methods *9*, 676–682.

Schnorrer, F., Kalchhauser, I., and Dickson, B.J. (2007). The transmembrane protein Kon-tiki couples to Dgrip to mediate myotube targeting in *Drosophila*. Dev. Cell *12*, 751–766.

Shimada, Y., Usui, T., Yanagawa, S., Takeichi, M., and Uemura, T. (2001). Asymmetric colocalization of Flamingo, a seven-pass transmembrane cadherin, and Dishevelled in planar cell polarization. Curr. Biol. *11*, 859–863.

Shulman, J.M., Perrimon, N., and Axelrod, J.D. (1998). Frizzled signaling and the developmental control of cell polarity. Trends Genet. *14*, 452–458.

Simons, M., and Mlodzik, M. (2008). Planar cell polarity signaling: from fly development to human disease. Annu. Rev. Genet. *42*, 517–540.

Strutt, D.I. (2001). Asymmetric localization of frizzled and the establishment of cell polarity in the *Drosophila* wing. Mol. Cell *7*, 367–375.

Strutt, H., and Strutt, D. (2008). Differential stability of flamingo protein complexes underlies the establishment of planar polarity. Curr. Biol. *18*, 1555–1564.

Taylor, J., Abramova, N., Charlton, J., and Adler, P.N. (1998). *Van Gogh*: a new Drosophila tissue polarity gene. Genetics *150*, 199–210.

Theisen, H., Purcell, J., Bennett, M., Kansagara, D., Syed, A., and Marsh, J.L. (1994). *Dishevelled* is required during *wingless* signaling to establish both cell polarity and cell identity. Development *120*, 347–360.

Tree, D.R.P., Shulman, J.M., Rousset, R., Scott, M.P., Gubb, D., and Axelrod, J.D. (2002). Prickle mediates feedback amplification to generate asymmetric planar cell polarity signaling. Cell *109*, 371–381.

Uemura, T., and Shimada, Y. (2003). Breaking cellular symmetry along planar axes in *Drosophila* and vertebrates. J. Biochem. *134*, 625–630.

Usui, T., Shima, Y., Shimada, Y., Hirano, S., Burgess, R.W., Schwarz, T.L., Takeichi, M., and Uemura, T. (1999). Flamingo, a seven-pass transmembrane cadherin, regulates planar cell polarity under the control of Frizzled. Cell *98*, 585–595.

Vega-Macaya, F., Manieu, C., Valdivia, M., Mlodzik, M., and Olguín, P. (2016). Establishment of the muscle-tendon junction during thorax morphogenesis in *Drosophila* requires the rho-kinase. Genetics *204*, 1139–1149.

Vinson, C.R., Conover, S., and Adler, P.N. (1989). A *Drosophila* tissue polarity locus encodes a protein containing seven potential transmembrane domains. Nature *338*, 263–264.

Wallingford, J.B. (2010). Planar cell polarity signaling, cilia and polarized ciliary beating. Curr. Opin. Cell Biol. *22*, 597–604.

Wilkin, M.B., Becker, M.N., Mulvey, D., Phan, I., Chao, A., Cooper, K., Chung, H.J., Campbell, I.D., Baron, M., and MacIntyre, R. (2000). *Drosophila* dumpy is a gigantic extracellular protein required to maintain tension at epidermal-cuticle attachment sites. Curr. Biol. *10*, 559–567.

Wolff, T., and Rubin, G.M. (1998). *Strabismus*, a novel gene that regulates tissue polarity and cell fate decisions in *Drosophila*. Development *125*, 1149–1159.

Wu, J., and Mlodzik, M. (2008). The frizzled extracellular domain is a ligand for Van Gogh/Stbm during nonautonomous planar cell polarity signaling. Dev. Cell *15*, 462–469.

Yang, C.H., Axelrod, J.D., and Simon, M.A. (2002). Regulation of Frizzled by fat-like cadherins during planar polarity signaling in the *Drosophila* compound eye. Cell *108*, 675–688.

Zallen, J.A. (2007). Planar polarity and tissue morphogenesis. Cell *129*, 1051–1063.

STAR★METHODS

KEY RESOURCES TABLE

REAGENT or RESOURCE	SOURCE	IDENTIFIER
Experimental models: Organisms/strains		
Drosophila melanogaster : *pnr*-Gal4 (MD237)	Bloomington Drosophila Stock Center.	BDSC#3039
Drosophila melanogaster: *w*[1118]	Bloomington Drosophila Stock Center.	BDSC#3605
Drosophila melanogaster: *shg* (E-cadherin)::GFP	Bloomington Drosophila Stock Center.	BDSC#60584
Drosophila melanogaster: sChMCA	Bloomington Drosophila Stock Center.	BDSC#35521
Drosophila melanogaster: *fz* [15]	(Jones et al., 1996)	N/A
Drosophila melanogaster: *fz* [P21]	(Jones et al., 1996)	N/A
Drosophila melanogaster: *ds* [UAO71]	(Adler et al., 1998)	N/A
Drosophila melanogaster: *ds* [38k]	(Clark et al., 1995)	N/A
Drosophila melanogaster: sGMCA	(Kiehart et al., 2000)	N/A
Drosophila melanogaster: *1151*-Gal4	(Roy and VijayRaghavan, 1997)	N/A
Drosophila melanogaster: UAS-N^{act}	(Go et al., 1998)	N/A
Drosophila melanogaster: YFP-trapped Dpy	Kyoto Stock Center (DGRC)	DGRC#115238
Drosophila melanogaster: UAS-*stbm*-IR	Bloomington Drosophila Stock Center.	BDSC#34354
Drosophila melanogaster: UAS-*chas*-IR	Vienna Drosophila Resource Center	VDRC#31766
Drosophila melanogaster: UAS-*dpy*-IR (strong RNAi line)	Vienna Drosophila Resource Center	VDRC#25933
Drosophila melanogaster: UAS-*dpy*-IR (weak RNAi line)	Vienna Drosophila Resource Center	VDRC#25823
Drosophila melanogaster: UAS-*baz*-IR	Vienna Drosophila Resource Center	VDRC#2914
Drosophila melanogaster: UAS-*kon-tiki* (*perdido*)-IR	National Institute of Genetics (NIG)	NIG#10275R-1
Drosophila melanogaster: *PBace01663*	The Exelixis Collection	#e01663
Drosophila melanogaster: *P[XP]d02121*	The Exelixis Collection	#d02121
Drosophila melanogaster: *chas*[NY1]	This paper	N/A
Software and algorithms		
ImageJ/FIJI	(Schindelin et al., 2012)	https://fiji.sc/
Adobe Photoshop	Adobe	https://www.adobe.com/products/photoshop.html
Adobe Illustrator	Adobe	https://www.adobe.com/products/illustrator.html
Stereonet 10	Richard Waldron Allmendinger	http://www.geo.cornell.edu/geology/faculty/RWA/programs/stereonet.html
Helicon Focus software	Helicon Soft	https://www.heliconsoft.com/heliconsoft-products/helicon-focus/
Prism 7 and 8	GraphPad	http://www.graphpad.com/

RESOURCE AVAILABILITY

Lead contact

Further information and requests for resources and reagents should be directed to and will be fulfilled by the lead contact, Masakazu Yamazaki (yamazaki@med.akita-u.ac.jp).

Materials availability

All reagents generated in this study are available from the lead contact.

Data and code availability

- All data reported in this study will be shared by the lead contact upon request.
- This paper does not report original code.
- Any additional information required to reanalyze the data reported in this paper is available from the lead contact upon request.

EXPERIMENTAL MODEL AND SUBJECT DETAILS

Drosophila strains and genetics

Flies were cultured using standard medium at 25°C unless otherwise stated. In this study, adult male flies (and male pupae) were used for mutant experiments, and female flies and pupae were used for RNAi experiments. RNAi studies were performed using the Gal4/UAS system (Brand and Perrimon, 1993). The following *Drosophila* strains were studied: *pnr*-Gal4 (MD237), w[1118] (used as the control), *shg* (E-cadherin)::GFP (Huang et al., 2009), and sChMCA (Abreu-Blanco et al., 2011) (all from the Bloomington Drosophila Stock Center); *fz* [15], *fz* [P21], *ds* [UAO71], and *ds* [38k] (all gifts from P. Adler); sGMCA (Kiehart et al., 2000) (a gift from D. Kiehart); *1151*-Gal4 (a gift from U. Nongthomba); UAS-N^{act} (a gift from S. Artavanis-Tsakonas); YFP-trapped Dpy (Lowe et al., 2014; Lye et al., 2014) (the Kyoto Stock Center); UAS-*stbm*-IR (34354) [from the Transgenic RNAi Project (TRiP)]; UAS-*chas*-IR (31766), UAS-*dpy*-IR (strong RNAi line, 25933; weak RNAi line, 25823), and UAS-*baz*-IR (2914) [all from Vienna Drosophila Resource Center (VDRC)]; and UAS-*kon-tiki* (*perdido*)-IR (10275R-1) [from National Institute of Genetics (NIG)]. The *chas* deletion allele was produced as previously described (Olguin et al., 2011) by the FLP-FRT-based deletion method (Parks et al., 2004) using *PBace01663* and *P[XP]d02121*. Proper deletion of the expected genomic region in this allele was confirmed by PCR and phenotypic analysis. Genotypes of the flies used in individual Figure panels are listed below.

Figure 1

(A, left) *white* (*w*)
(A, right) fz^{15}/fz^{P21}
(B, left) *pnr*-Gal4/+
(B, right) *pnr*-Gal4/UAS-*stbm*-IR (34354, TRiP)
(Ci, Di and Ei) sGMCA/+; *pnr*-Gal4/+
(Cii, Dii and Eii) sGMCA/+; *pnr*-Gal4, UAS-*stbm*-IR (34354, TRiP)/+

Figure 2

(Ci and Di) *1151*-Gal4/*Y*; *shg*::GFP/+
(Cii and Dii) *1151*-Gal4/*Y*; *shg*::GFP/+; fz^{15}/fz^{P21}

Figure 3

(Ai and Ai') *1151*-Gal4/*Y*
(Aii and Aii') *1151*-Gal4, $chas^{NY1}/Y$
(Aiii and Aiii') *1151*-Gal4/*Y*;; fz^{15}/fz^{P21}
(Aiv and Aiv') *1151*-Gal4, $chas^{NY1}/Y$;; fz^{15}/fz^{P21}
(Av and Av') *1151*-Gal4/*Y*; UAS-N^{intra}/+
(Avi and Avi') *1151*-Gal4, $chas^{NY1}/Y$; UAS-N^{intra}/+
(Avii and Avii') *1151*-Gal4/*Y*; UAS-N^{intra}/+; fz^{15}/fz^{P21}
(Aviii and Aviii') *1151*-Gal4, $chas^{NY1}/Y$; UAS-N^{intra}/+; fz^{15}/fz^{P21}. (Bi and Ci) *1151*-Gal4, $chas^{NY1}/Y$; *shg*::GFP/+; fz^{15}/fz^{P21}. (Bii and Cii) *1151*-Gal4, $chas^{NY1}/Y$; *shg*::GFP, UAS-N^{intra}/+; fz^{15}/fz^{P21}

Figure 4

(Ai) ds^{UAO71}/ds^{38K}
(Aii) ds^{UAO71}/ds^{38K}; *pnr*-Gal4, UAS-*chas*-IR (31766, VDRC), UAS-*stbm*-IR (34354, TRiP)/+
(Bi, Ci and Di) *shg*::GFP/+
(Bii, Cii and Dii) ds^{UAO71}, *shg*::GFP/ ds^{38K}

Figure 5. (Bi and Ci) *shg*::GFP/+; *pnr*-Gal4/+

(Bii and Cii) *shg*::GFP/+; *pnr*-Gal4, UAS-*stbm*-IR (34354, TRiP)/+

(Di) *1151*-Gal4/*Y*; *shg*::GFP/+
(Dii) *1151*-Gal4/*Y*; *shg*::GFP/+; fz^{15}/fz^{P21}

Figure 6. (B and C) *1151*-Gal4/*Y*; *shg*::GFP/+; fz^{15}/fz^{P21}

(Di) sGMCA/+; *pnr*-Gal4, UAS-*stbm*-IR (34354, TRiP)/+
(Dii) sGMCA/+; *pnr*-Gal4, UAS-*chas*-IR (31766, VDRC), UAS-*stbm*-IR (34354, TRiP)/+

Figure 7

(A, left) *dpy*::YFP/+; *pnr*-Gal4, UAS-*chas*-IR (31766, VDRC), UAS-*stbm*-IR (34354, TRiP)/sChMCA
(A, right) *dpy*::YFP/+; sChMCA/+
(Bi, Ci and Di) sGMCA/+; *pnr*-Gal4, UAS-*chas*-IR (31766, VDRC), UAS-*stbm*-IR (34354, TRiP)/+
(Bii, Cii and Dii) sGMCA/*dpy*-IR (25933, VDRC); *pnr*-Gal4, UAS-*chas*-IR (31766, VDRC), UAS-*stbm*-IR (34354, TRiP)/+
(Ei) UAS-*dpy*-IR (25933, VDRC)/+; *pnr*-Gal4/+
(Eii) *pnr*-Gal4, UAS-*chas*-IR (31766, VDRC), UAS-*stbm*-IR (34354, TRiP)/+
(Eiii) UAS-*dpy*-IR (25933, VDRC)/+; *pnr*-Gal4, UAS-*chas*-IR (31766, VDRC), UAS- *stbm*-IR (34354, TRiP)/+
(F, left) *pnr*-Gal4, UAS-*chas*-IR (31766, VDRC), UAS-*stbm*-IR (34354, TRiP)/+
(F, right) UAS-*dpy*-IR (25933, VDRC)/+; *pnr*-Gal4, UAS-*chas*-IR (31766, VDRC), UAS-*stbm*-IR (34354, TRiP)/+

Figure S1

(Ai, Bi and Ci) *1151*-Gal4/*Y*; *shg*::GFP/+
(Aii, Bii and Cii) *1151*-Gal4/*Y*; *shg*::GFP, UAS-N^{intra}/+
(Aiii, Biii and Ciii) *1151*-Gal4/*Y*; *shg*::GFP/+; fz^{15}/fz^{P21}
(Aiv, Biv and Civ) *1151*-Gal4/*Y*; *shg*::GFP, UAS-N^{intra}/+; fz^{15}/fz^{P21}
(Av, Bv and Cv) *1151*-Gal4, $chas^{NY1}/Y$; *shg*::GFP/+; fz^{15}/fz^{P21}
(Avi, Bvi and Cvi) *1151*-Gal4, $chas^{NY1}/Y$; *shg*::GFP, UAS-N^{intra}/+; fz^{15}/fz^{P21}

Figure S2

(A, A' and A") *pnr*-Gal4/+
(B, B' and B") *pnr*-Gal4/UAS-*stbm*-IR (34354, TRiP)
(C, C' and C") *pnr*-Gal4/UAS-*chas*-IR (31766, VDRC)
(D, D' and D") *pnr*-Gal4, UAS-*chas*-IR (31766, VDRC), UAS-*stbm*-IR (34354, TRiP)/+
(Ei, Fi and Fii) *shg*::GFP/+; *pnr*-Gal4/+
(Eii, Fiii and Fiv) *shg*::GFP/+; *pnr*-Gal4, UAS-*stbm*-IR (34354, TRiP)/+
(Eiii, Fv and Fvi) *shg*::GFP/+; *pnr*-Gal4, UAS-*chas*-IR (31766, VDRC)/+
(Eiv, Fvii and Fviii) *shg*::GFP/+; *pnr*-Gal4, UAS-*chas*-IR (31766, VDRC), UAS-*stbm*-IR (34354,TRiP)/+

Figure S3

(i and ii) *shg*::GFP/+; *pnr*-Gal4/+
(iii and iv) *shg*::GFP/+; *pnr*-Gal4, UAS-*stbm*-IR (34354, TRiP)/+
(v and vi) *shg*::GFP/+; *pnr*-Gal4, UAS-*chas*-IR (31766, VDRC)/+
(vii and viii) *shg*::GFP/+; *pnr*-Gal4, UAS-*chas*-IR (31766, VDRC), UAS-*stbm*-IR (34354, TRiP)/+

Figure S4

(Ai, Bi, Bii, Ci and Cii) *1151*-Gal4/*Y*; *shg*::GFP/+
(Aii, Biii, Biv, Ciii and Civ) *1151*-Gal4/*Y*; *shg*::GFP/+; fz^{15}/fz^{P21}
(Ei) *1151*-Gal4/*Y*;; UAS-*kon-tiki*-IR /+
(Eii) *1151*-Gal4, $chas^{NY1}/Y$;; UAS-*kon-tiki*-IR /+
(Eiii) *1151*-Gal4/*Y*;; UAS-*kon-tiki*-IR, fz^{15}/fz^{P21}
(Eiv) *1151*-Gal4, $chas^{NY1}/Y$;; UAS-*kon-tiki*-IR, fz^{15}/fz^{P21}

Figure S5

(Ai, B and B') UAS-*baz*-IR (2914, VDRC)/+; *pnr*-Gal4/+
(Aii, C and C') UAS-*baz*-IR (2914, VDRC)/+; *pnr*-Gal4, UAS-*chas*-IR (31766, VDRC), UAS-*stbm*-IR (34354, TRiP)/+
(Di) sGMCA/+; *pnr*-Gal4, UAS-*stbm*-IR (34354, TRiP)/+
(Dii) sGMCA/+; *pnr*-Gal4, UAS-*chas*-IR (31766, VDRC), UAS-*stbm*-IR (34354, TRiP)/+

Figure S6

(Ai, Aiv and Avii) *dpy*::YFP/+; *pnr*-Gal4/sChMCA
(Aii, Av and Aviii) *dpy*::YFP/+; *pnr*-Gal4, UAS-*stbm*-IR (34354, TRiP)/sChMCA
(Aiii, Avi and Aix) *dpy*::YFP/+; *pnr*-Gal4, UAS-*chas*-IR (31766, VDRC), UAS-*stbm*-IR (34354, TRiP)/sChMCA
(B and C) sGMCA/+; *pnr*-Gal4, UAS-*chas*-IR (31766, VDRC), UAS-*stbm*-IR (34354, TRiP)/+
(D, left) sGMCA/+; *pnr*-Gal4, UAS-*chas*-IR (31766, VDRC), UAS-*stbm*-IR (34354, TRiP)/+
(D, right) sGMCA/UAS-*dpy*-IR (25933, VDRC); *pnr*-Gal4, UAS-*chas*-IR (31766, VDRC), UAS-*stbm*-IR (34354, TRiP)/+

Figure S7

(Ai, Bi, Ci and Di) *shg*::GFP/+; *pnr*-Gal4, UAS-*chas*-IR (31766, VDRC), UAS-*stbm*-IR (34354,TRiP)/+
(Aii, Bii, Cii and Dii) *shg*::GFP/UAS-*dpy*-IR (25933, VDRC); *pnr*-Gal4, UAS-*chas*-IR (31766, VDRC), UAS-*stbm*-IR (34354,TRiP)/+
(Ei) UAS-*dpy*-IR (25933, VDRC)/+; *pnr*-Gal4/+
(Eii) UAS-*dpy*-IR (25823, VDRC)/+; *pnr*-Gal4/+
(Fi and Fi') UAS-*dpy*-IR (25933, VDRC)/+; *pnr*-Gal4/UAS-*stbm*-IR (34354, TRiP)
(Fii and Fii') UAS-*dpy*-IR (25823, VDRC)/+; *pnr*-Gal4/UAS-*stbm*-IR (34354, TRiP)
(Gi and Gi') *1151*-Gal4; dpy^{ov1}/dpy^{ov1}
(Gii and Gii') *1151*-Gal4, $chas^{NY1}/Y$; dpy^{ov1}/dpy^{ov1}
(Giii and Giii') UAS-*dpy*-IR (25933, VDRC)/+; *pnr*-Gal4, UAS-*chas*-IR (31766, VDRC)/+
(Giv and Giv') UAS-*dpy*-IR (25823, VDRC)/+; *pnr*-Gal4, UAS-*chas*-IR (31766, VDRC)/+

METHOD DETAILS

Live imaging analysis

Preparation of live *Drosophila* pupae for time-lapse imaging was performed essentially as described previously (Koto et al., 2009; Mauri et al., 2014). Briefly, pupae were fixed on a glass slide using double-sided tape. The pupal case covering the head and notum was carefully removed. A ring of silicon vacuum grease (Shinetsu) was drawn around the pupa on the glass slide, and then a glass coverslip was placed on the ring of silicon to seal the chamber. Before sealing, a small drop of Immersol W 2010 (Zeiss) was placed between the coverslip surface and the notum to bring them into contact.

Pupae in chambers were imaged at 25 ± 1°C for 5–16 h with an inverted confocal microscope (LSM780, Zeiss) equipped with a 63× oil immersion lens (Plan-Apochromat 63×/1.40 Oil DIC M27, Zeiss). Time-lapse images of E-cadherin::GFP pupae (Z-stacks, 45–62 slices taken at 0.57 μm depth intervals) were acquired at 5 min intervals using the normal mode (for single-position movies) or the tile scan mode [for multi-position (4 positions) tile movies]. Single-position movies of sGMCA pupae were acquired at 10 min intervals (50–75 slices, 0.37 μm/slice). In the case of sGMCA pupae in which *dpy* was depleted, the image acquisition conditions were changed to 300 slices and 20 min intervals due to the dent formed in the notum epithelium. Using the aDC bristle as a landmark for all experiments, the area to be imaged was selected and fixed throughout imaging. Photobleaching experiments were performed by scanning at 488 nm laser with a 63× oil immersion lens (Plan-Apochromat 63×/1.40 Oil DIC M27, Zeiss). Bleached regions were of identical geometry. After photobleaching at 24 hAPF, time-lapse images of pupae expressing *dpy*::YFP and sChMCA were acquired at 10 min intervals (50–75 slices, 0.37 μm/slice). All pupae used in live imaging experiments were able to develop to at least the eclosion stage.

Analysis of time-lapse images

All movies in this study are maximum intensity projections of Z-stacks produced using ImageJ/FIJI. Stitching for multi-position tile movies was performed using ImageJ/FIJI. For quantitative analyses, the 5 min interval frames of the original time-lapse series were subtracted to make a series of sequential images at 10 min intervals.

The velocity and orientation of tissue flows were measured by manually tracking the socket cells using the ImageJ/FIJI plugin "MTrackJ". The position of the bristle cell in the ES organ and the angles of developing pupal bristles (in sGMCA live imaging) and adult bristles were measured using ImageJ/FIJI. For quantitative and statistical analyses, the above data for microchaeta, but not macrochaeta (aDC bristles), in the region of interest were used. Images were processed using FIJI and Adobe Photoshop 2021.

Histological analyses

The nota of adult flies were imaged using a stereomicroscope (Stemi 2000, Zeiss) equipped with a digital camera (EOS Kiss X6i, Canon). Adult fly cuticles were prepared as previously described (Ayukawa et al., 2014). Digital images and cuticle preparation images were processed from multiple image stacks using Helicon Focus software (Helicon Soft) and Adobe Photoshop 2021 as previously described (Ayukawa et al., 2014).

QUANTIFICATION AND STATISTICAL ANALYSIS

Stereonet 10 (http://www.geo.cornell.edu/geology/faculty/RWA/programs/stereonet.html) and Adobe Illustrator 2021 were used to draw rose diagrams. Rose diagrams are composed of 18 bins of 20° each. The innermost circle represents 20% and the concentric circles in each rose diagram indicate 20% increments. The total number of bristles, socket cells or bristle-socket pairs analyzed (N), and the number of pupae or adult files that were used for each quantitative analysis (in parentheses), are shown in each figure panel.

Prism 7 and 8 (GraphPad) were used for statistical analyses. Two-sided p values were calculated using the Mann-Whitney test, Kruskal Wallis test with Dunn's multiple comparison test or Fisher's exact test, and $p < 0.05$ was considered to indicate statistical significance. "n.s." means not statistically significant.